Plant Communications
Research article

CellPress
Partner Journal

ABI5–FLZ13 module transcriptionally represses growth-related genes to delay seed germination in response to ABA

Chao Yang[1,2,*], Xibao Li[2], Shunquan Chen[2], Chuanliang Liu[2], Lianming Yang[2], Kailin Li[2], Jun Liao[2], Xuanang Zheng[2], Hongbo Li[2], Yongqing Li[1], Shaohua Zeng[1], Xiaohong Zhuang[3], Pedro L. Rodriguez[4], Ming Luo[1,*], Ying Wang[1,*] and Caiji Gao[2,*]

[1]Key Laboratory of South China Agricultural Plant Molecular Analysis and Genetic Improvement & Guangdong Provincial Key Laboratory of Applied Botany, South China Botanical Garden, Chinese Academy of Sciences, Guangzhou 510650, China

[2]Guangdong Provincial Key Laboratory of Biotechnology for Plant Development, School of Life Sciences, South China Normal University (SCNU), Guangzhou 510631, China

[3]School of Life Sciences, Centre for Cell and Developmental Biology, The Chinese University of Hong Kong, Shatin, New Territories, Hong Kong, China

[4]Instituto de Biología Molecular y Celular de Plantas, Consejo Superior de Investigaciones Científicas-Universidad Politécnica de Valencia, 46022 Valencia, Spain

***Correspondence: Chao Yang (chaoyang@scbg.ac.cn), Ming Luo (luoming@scbg.ac.cn), Ying Wang (yingwang@scib.ac.cn), Caiji Gao (gaocaiji@m.scnu.edu.cn)**

https://doi.org/10.1016/j.xplc.2023.100636

ABSTRACT

The bZIP transcription factor ABSCISIC ACID INSENSITIVE5 (ABI5) is a master regulator of seed germination and post-germinative growth in response to abscisic acid (ABA), but the detailed molecular mechanism by which it represses plant growth remains unclear. In this study, we used proximity labeling to map the neighboring proteome of ABI5 and identified FCS-LIKE ZINC FINGER PROTEIN 13 (FLZ13) as a novel ABI5 interaction partner. Phenotypic analysis of *flz13* mutants and *FLZ13*-overexpressing lines demonstrated that FLZ13 acts as a positive regulator of ABA signaling. Transcriptomic analysis revealed that both FLZ13 and ABI5 downregulate the expression of ABA-repressed and growth-related genes involved in chlorophyll biosynthesis, photosynthesis, and cell wall organization, thereby repressing seed germination and seedling establishment in response to ABA. Further genetic analysis showed that FLZ13 and ABI5 function together to regulate seed germination. Collectively, our findings reveal a previously uncharacterized transcriptional regulatory mechanism by which ABA mediates inhibition of seed germination and seedling establishment.

Key words: ABA, ABI5, FLZ, gene expression, seed germination

Yang C., Li X., Chen S., Liu C., Yang L., Li K., Liao J., Zheng X., Li H., Li Y., Zeng S., Zhuang X., Rodriguez P.L., Luo M., Wang Y., and Gao C. (2023). ABI5–FLZ13 module transcriptionally represses growth-related genes to delay seed germination in response to ABA. Plant Comm. **4**, 100636.

INTRODUCTION

Abscisic acid (ABA), a sesquiterpene compound discovered in the 1960s (Eagles and Wareing, 1963; Ohkuma et al., 1963; Cornforth et al., 1965; Addicott et al., 1968), is important for plant stress tolerance, growth, and development (Leung and Giraudat, 1998; Holdsworth et al., 2008; Cutler et al., 2010; Chen et al., 2020). ABA is perceived by the soluble ABA receptor PYRABACTIN RESISTANCE1 (PYR1)/PYR1-LIKE (PYL)/REGULATORY COMPONENT OF ABA RECEPTOR (RCAR) (Ma et al., 2009; Nishimura et al., 2009; Park et al., 2009; Santiago et al., 2009). Upon ABA binding, these receptors can form a complex with TYPE 2C PROTEIN PHOSPHATASES (PP2Cs), thereby relieving PP2C inhibition of SUCROSE NONFERMENTING-1-RELATED PROTEIN KINASE 2s (SnRK2s) from subfamily III, including SnRK2.2, SnRK2.3, and SnRK2.6 (Ma et al., 2009; Miyazono et al., 2009; Nishimura et al., 2009; Park et al., 2009; Cutler et al., 2010; Chen et al., 2020). In addition, B2- and B3-type Raf protein kinases directly phosphorylate and activate subclass III SnRK2s (Saruhashi et al., 2015; Nguyen et al., 2019; Katsuta et al., 2020; Takahashi

Published by the Plant Communications Shanghai Editorial Office in association with Cell Press, an imprint of Elsevier Inc., on behalf of CSPB and CEMPS, CAS.

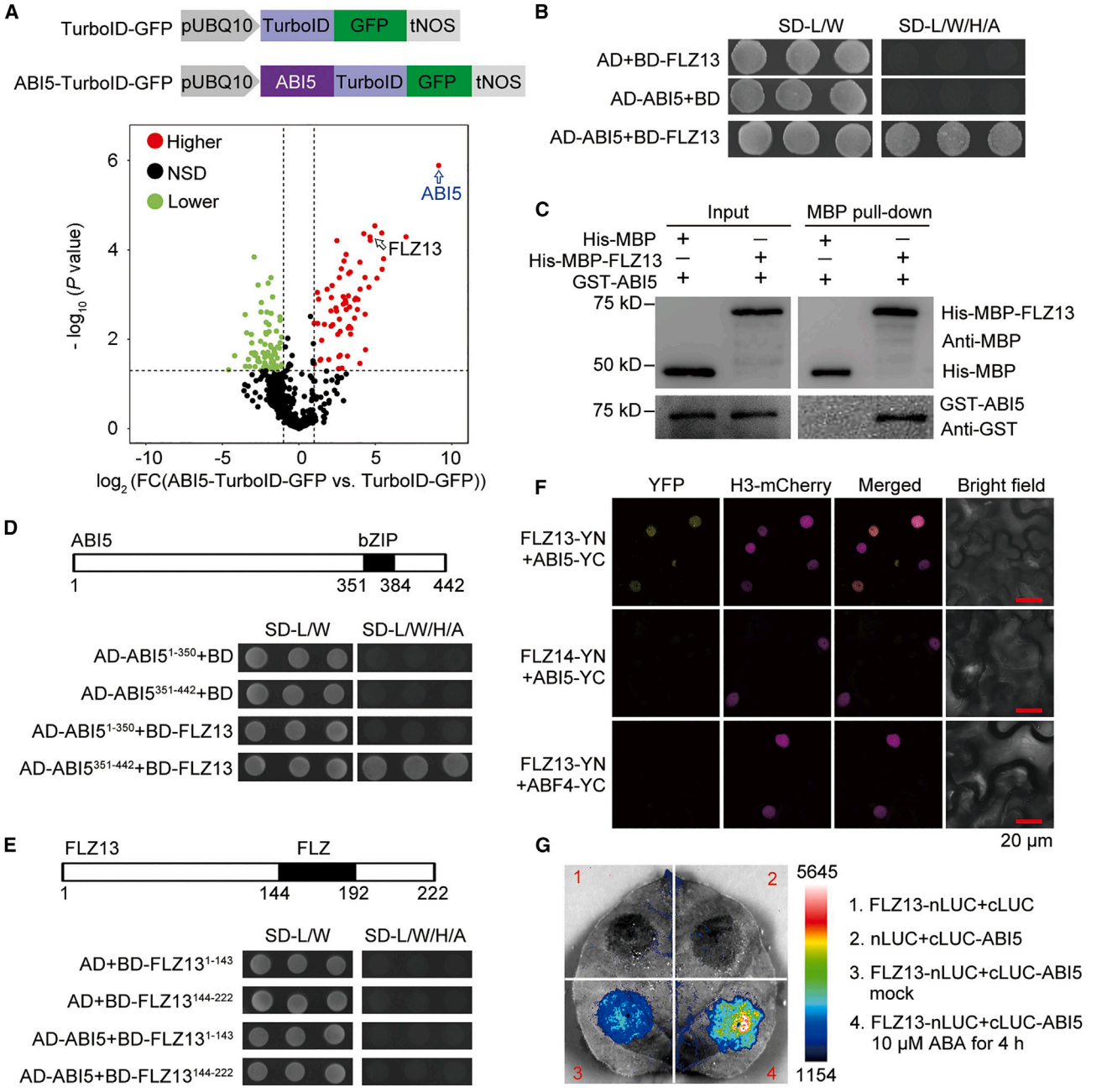

Figure 1. Identification of FLZ13 as a novel interactor of ABI5.

(A) Volcano plot showing protein abundances in the ABI5-TurboID-GFP vs. TurboID-GFP pair. The constructs encoding the ABI5-TurboID-GFP and TurboID-GFP fusion proteins are shown. Integrated label-free quantitation (LFQ) peptide intensity data from three biological replicates of each sample were normalized and subjected to ratiometric analysis and plotting using the Perseus program. In total, 611 proteins identified in both the ABI5-TurboID-GFP and TurboID-GFP samples were plotted. Preys with fold change >2 ($\log_2$(FC) > 1) and $P < 0.05$ ($-\log_{10}$[P value] > 1.301) are indicated by colored dots. Green and red dots represent significantly decreased and increased protein levels, respectively. NSD stands for no significant difference.

(B) Y2H assay showing the interaction between ABI5 and FLZ13. Protein interactions were determined by growth of yeast cells co-transformed with various combinations of plasmids on synthetic dropout medium lacking Leu and Trp (SD-L/W) and lacking Leu, Trp, His, and Ade (SD-L/W/H/A), as indicated.

(C) *In vitro* pull-down assay showing physical binding of ABI5 and FLZ13. Equal amounts of GST-ABI5 were incubated with His-MBP and His-MBP-FLZ13 bound to MBP magnetic beads and then eluted and analyzed by immunoblotting using anti-GST and anti-MBP antibodies.

(D and E) Mapping of the interaction region of ABI5 and FLZ13 by Y2H. Diagrams of the ABI5 **(D)** and FLZ13 **(E)** protein structures are shown. Protein interactions were determined by growth of yeast cells co-transformed with various combinations of plasmids on synthetic dropout medium lacking Leu and Trp (SD-L/W) and lacking Leu, Trp, His, and adenine (SD-L/W/H/A), as indicated.

(legend continued on next page)

et al., 2020; Lin et al., 2021). Activated SnRK2s phosphorylate and activate downstream transcription factors such as ABA-responsive element (ABRE)-binding protein/ABRE-binding factors (AREB/ABFs), which subsequently modulate the expression of ABA-responsive genes (Kobayashi et al., 2005; Furihata et al., 2006; Fujii et al., 2007; Fujii and Zhu, 2009; Nakashima et al., 2009).

ABA INSENSITIVE 5 (ABI5), a bZIP transcription factor that is preferentially expressed in dry seeds and strongly induced by exogenous ABA, plays a critical role in ABA-mediated seed germination and post-germinative growth in *Arabidopsis* (Finkelstein, 1994; Finkelstein and Lynch, 2000; Lopez-Molina and Chua, 2000; Lopez-Molina et al., 2001, 2002; Brocard et al., 2002; Finkelstein et al., 2005; Yu et al., 2015; Skubacz et al., 2016). *ABI5* loss-of-function mutants are hyposensitive to ABA, whereas plants overexpressing *ABI5* display hypersensitivity to ABA (Finkelstein, 1994; Finkelstein and Lynch, 2000; Lopez-Molina and Chua, 2000; Zhou et al., 2015). As a transcription factor, ABI5 functions mainly by modulating the expression of its target genes (Skubacz et al., 2016). Previous studies have identified thousands of ABI5-targeted genes (Lee et al., 2012; Nakabayashi et al., 2005; Nakashima et al., 2009; Reeves et al., 2011; O'Malley et al., 2016); however, the detailed functions of these genes in ABA-regulated seed germination remain elusive. For example, *EARLY METHIONINE-LABELED 6* (*Em6*) is a well-known ABA-induced target gene of ABI5 (Carles et al., 2002), but the *em6-1* mutant does not display an obvious defect in ABA-repressed seed germination (Manfre et al., 2006). Recently, Huang et al. reported that *PHOSPHATE1* (*PHO1*), an important regulator of phosphorus transport in *Arabidopsis* (Hamburger et al., 2002), is an ABA-repressed gene that is targeted by ABI5 to control seed germination (Huang et al., 2017). Although loss-of-function mutations in *PHO1* completely abolish the ABA-hyposensitive phenotype of the *abi5-8* mutant (Zhou et al., 2015), the function of *PHO1* in ABA-inhibited seed germination remains unknown (Huang et al., 2017). Thus, the mechanisms underlying ABI5-mediated ABA responses during seed germination and seedling establishment require further characterization.

ABI5 is often associated with other transcriptional regulators, such as ABI3, DELLA, BRI1-EMS-SUPPRESSOR1 (BES1), JASMONATE ZIM-DOMAIN (JAZ) proteins, VQ18/26, and INDUCER OF CBF EXPRESSION1 (ICE1), to regulate ABA responses (Lim et al., 2013; Pan et al., 2018; Hu et al., 2019; Ju et al., 2019; Zhao et al., 2019). Most of the aforementioned interactors function as negative regulators to suppress the transcriptional regulatory activity of ABI5, whereas the positive regulators of ABI5 are less well understood. Several studies have demonstrated the formation of an ABI3–ABI5 complex to activate downstream genes containing ABREs (Nakamura et al., 2001; Gampala et al., 2002; Finkelstein et al., 2005), and other studies have suggested that ABI5 can act as a transcription factor without ABI3 (Lopez-Molina et al., 2002). Thus, ABI5 can rescue the *abi3-1* mutant and act downstream of ABI3 to induce growth arrest (Lopez-Molina et al., 2002). Recently, the circadian clock proteins PSEUDO-RESPONSE REGULATOR 5 (PRR5) and PRR7 were found to interact with and stimulate ABI5 to positively modulate ABA signaling during seed germination (Yang et al., 2021). Despite these findings, details of the transcriptional regulatory mechanisms of ABI5 and its cofactors remain to be fully characterized.

Previous studies have reported that endospermic ABA represses expression of cutin biosynthetic genes in the embryo through ABI5 action, which favors ABA-mediated inhibition of the embryo-to-seedling transition (De Giorgi et al., 2015). Our recent study revealed that the plant-specific endosomal sorting complex required for transport (ESCRT) component FYVE DOMAIN PROTEIN REQUIRED FOR ENDOSOMAL SORTING 1 (FREE1) physically interacts with ABI5 and interferes with its DNA-binding ability to negatively regulate seedling establishment in the presence of ABA (Li et al., 2019, 2022a). To gain further insight into the mechanism of ABI5-engaged transcriptional regulation, we used TurboID, an enzyme with high activity in protein proximity labeling (Mair et al., 2019), to map the neighboring proteome of ABI5 and identified a hitherto unknown ABI5-interacting protein, FCS-LIKE ZINC FINGER PROTEIN 13 (FLZ13). Further studies showed that FLZ13 functions together with ABI5 to determine the transcription of ABA-repressed and growth-related genes, thus positively modulating ABA responses during seed germination and post-germinative growth.

RESULTS

Proximity labeling proteomics identifies FLZ13 as a novel ABI5-interacting protein

To map the neighboring proteome of ABI5, we generated transgenic plants expressing either the ABI5-TurboID-GFP fusion or TurboID-GFP as a control in the Col-0 background (Figure 1A). The ABI5-TurboID-GFP fusion was functional *in planta*, because ABI5-TurboID-GFP was correctly localized in the nucleus and its overexpressing seedlings were hypersensitive to 0.5 μM ABA treatment compared with the *TurboID-GFP* plants (Supplemental Figure 1). Five-day-old seedlings were incubated with 100 μM ABA for 4 h, then treated with 50 μM biotin for another 1 h before being harvested to isolate total proteins for affinity purification with streptavidin-coated beads, followed by label-free quantitative mass spectrometry. Using P value <0.05 and fold change >2 as cutoffs, we obtained 67 ABI5-specific prey (Figure 1A; Supplemental Table 1). Among them, ABI5 BINDING PROTEIN1 (AFP1) and FREE1 were previously reported as ABI5-interacting proteins (Lopez-Molina et al., 2003; Garcia et al., 2008; Li et al., 2019), indicating that our TurboID-based proximity labeling was effective in isolating ABI5 interactors. To gain an overview of these candidates, 48

(F) BiFC assay revealing the association between ABI5 and FLZ13 in the nuclei of *N. benthamiana* leaves. FLZ13 fused to the N-terminal half of YFP (FLZ13-YN) was co-infiltrated with ABI5 fused to the C-terminal half of YFP (ABI5-YC). The FLZ14-YN/ABI5-YC and FLZ13-YN/ABF4-YC pairs were used as negative controls. H3, histone 3.

(G) LCI assay showing the interaction between ABI5 and FLZ13 in *N. benthamiana* leaves. *Agrobacteria* harboring FLZ13-nLUC (N-terminal part of luciferase) were co-infiltrated with *Agrobacteria* harboring cLUC-ABI5 into *N. benthamiana* leaves. FLZ13-nLUC/cLUC and cLUC-ABI5/nLUC pairs were used as negative controls. After 36 h of co-infiltration, leaves were treated with mock and 10 μM ABA for 4 h, followed by luminescence imaging.

nuclear-localized proteins out of the 67 highly enriched proteins were used to construct a protein–protein interaction (PPI) network to show the known interlinks among them (Supplemental Table 2). As shown in Supplemental Figure 2A, 44 of 48 nuclear proteins were included in this network, indicating that they were indeed associated in plant cells. To enrich the ABI5-interacting network, a broader network was generated using the 48 nuclear proteins identified in this study with 37 known ABI5-interacting proteins (Supplemental Table 3). Eighty-two out of 83 unique proteins could be connected in this network (Supplemental Figure 2B), indicating that ABI5 potentially associated with diverse proteins to generate multiple functional complexes and that TurboID-based proximity labeling is a powerful approach for identifying the protein interactome in plants.

Among the ABI5-neighboring proteins identified in this study, FLZ13 is the most interesting because its gene expression is induced by ABA (Supplemental Table 2) and its molecular function has not been characterized. FLZs are a group of plant-specific regulatory proteins containing a common FCS-LIKE ZINC FINGER domain (FLZ; also known as Domain of Unknown Function 581) (Jamsheer and Laxmi, 2015) whose biological functions are just beginning to be explored. Therefore, we chose FLZ13 as an example and characterized its function in the ABI5-mediated signaling pathway. Yeast two-hybrid (Y2H) analysis showed that FLZ13 could specifically interact with ABI5 but not with other transcription factors in ABA signaling, including ABI3, ABI4, ABF2, and ABF4 (Figure 1B and SupplementalFigure 3). The direct interaction between FLZ13 and ABI5 was further corroborated by an *in vitro* pull-down assay in which GST-ABI5 was specifically precipitated by His-MBP-FLZ13 but not by His-MBP alone (Figure 1C). Additional Y2H assays with truncated proteins showed that the C-terminal part of ABI5 (351–442 amino acids) harboring a bZIP domain, but not the N-terminal part of ABI5 (1–350 amino acids), was able to bind FLZ13 (Figure 1D). Furthermore, truncated FLZ13 lacking either the N-terminal or C-terminal half failed to interact with ABI5 (Figure 1E). These Y2H results suggest that the C-terminal bZIP domain of ABI5 mediates its interaction with full-length FLZ13. To confirm the interaction between ABI5 and FLZ13 *in planta*, we performed bimolecular fluorescence complementation (BiFC) and luciferase complementation imaging (LCI) assays. The BiFC results revealed that ABI5 interacted with FLZ13 in the nucleus (Figure 1F). Furthermore, co-expression of FLZ13-nLUC with cLUC-ABI5 in tobacco leaves resulted in obvious LUC signals (Figure 1G and Supplemental Figure 4) that were significantly increased by ABA treatment, indicating that ABA may promote the formation of the ABI5–FLZ13 complex (Figure 1G and Supplemental Figure 4). Collectively, these results clearly demonstrate that FLZ13 physically interacts with ABI5, suggesting that FLZ13 might function as a working partner of ABI5 to modulate ABA signaling.

FLZ13 is responsive to ABA in germinating seeds and positively regulates ABA response

Given that FLZ13 is a novel interactor of ABI5, we examined the transcription and protein expression of *FLZ13* during seed germination with or without exogenous ABA treatment. Consistent with previous reports (Lopez-Molina et al., 2001; Brocard et al., 2002), the transcription of *ABI5* decreased substantially following seed germination but increased upon 0.5 μM ABA treatment (Supplemental Figures 5A and 5B). However, *FLZ13* displayed a slightly increased expression pattern during seed germination and ABA treatment (Supplemental Figures 5A and 5B). To determine the protein abundance of ABI5 and FLZ13 in germinating seeds, we generated transgenic *Arabidopsis* lines expressing a *pFLZ13::FLZ13-GFP* fusion in the Col-0 background. As presented in Supplemental Figure 5C, the ABI5 protein showed remarkably decreased expression following seed germination, whereas the FLZ13-GFP protein displayed a gradual accumulation. When germinating seeds were exposed to 0.5 μM ABA, the protein levels of FLZ13-GFP did not change significantly compared with the control group (0 μM ABA), whereas ABI5 levels clearly increased (Supplemental Figure 5C). These results indicate the co-existence of FLZ13 and ABI5 in the presence of ABA, meeting the requirement for their interaction *in planta*.

The biological function of *FLZ13* in *Arabidopsis* has not yet been documented. As FLZ13 physically interacts with ABI5 (Figure 1) and responds to ABA in germinating seeds (Supplemental Figure 5), we hypothesized that FLZ13 might be involved in ABI5-mediated ABA signaling during seed germination. To test this possibility, we first generated *FLZ13* overexpression (OE) transgenic plants in the Col-0 background. Two representative homozygous lines (*pUBQ10::FLZ13-GFP* #1 and *pUBQ10::FLZ13-GFP* #*4*, termed *FLZ13*-OE #1 and OE #4) with higher *FLZ13* gene expression levels under normal growth conditions were chosen for further study (Supplemental Figure 6). As shown in Figure 2A–2C, seed germination and seedling growth of wild-type (WT) and *FLZ13*-OE lines did not show obvious differences in medium without exogenous ABA, whereas seeds of *FLZ13*-OE lines had much lower germination and greening rates than Col-0 in the presence of ABA, suggesting that overexpression of *FLZ13* conferred ABA hypersensitivity on seed germination and seedling establishment. We also overexpressed *FLZ13* in *pyr1pyl1pyl2pyl4pyl5pyl8* (*pyr1pyl12458*) and *snrk2.2snrk2.3* backgrounds for genetic analysis of FLZ13 and other components involved in ABA signaling (Fujii et al., 2007; Gonzalez-Guzman et al., 2012). The *FLZ13*-OE/*pyr1pyl12458* and *FLZ13*-OE/*snrk2.2snrk2.3* lines almost phenocopied the *pyr1pyl12458* and *snrk2.2snrk2.3* mutants, respectively (Figure 2D and 2E), suggesting that a functional ABA signaling pathway is required to show the effects of *FLZ13* overexpression on ABA hypersensitivity.

To further confirm the role of *FLZ13* in ABA signaling, we obtained an *FLZ13* transfer DNA insertion mutant (*flz13-1*, SALK_142112C) harboring a transfer DNA insertion 100 base pairs upstream of the 5′ untranslated region (UTR), which resulted in an obvious reduction (∼20% of WT expression) in the transcript level of *FLZ13* (Supplemental Figure 6). An ABA sensitivity test showed that the *flz13-1* mutant was slightly more resistant to ABA than Col-0 in terms of seed germination rate (Figures 2F and 3A). Next, we introduced a construct containing the entire genomic sequence of *FLZ13* into the *flz13-1* mutant (Supplemental Figure 6), resulting in 1.9-fold (*flz13-C* #3) and 2.38-fold (*flz13-C* #8) expression of *FLZ13*. Phenotype analysis showed that the two independent complementation lines germinated like WT plants in response to 0.5

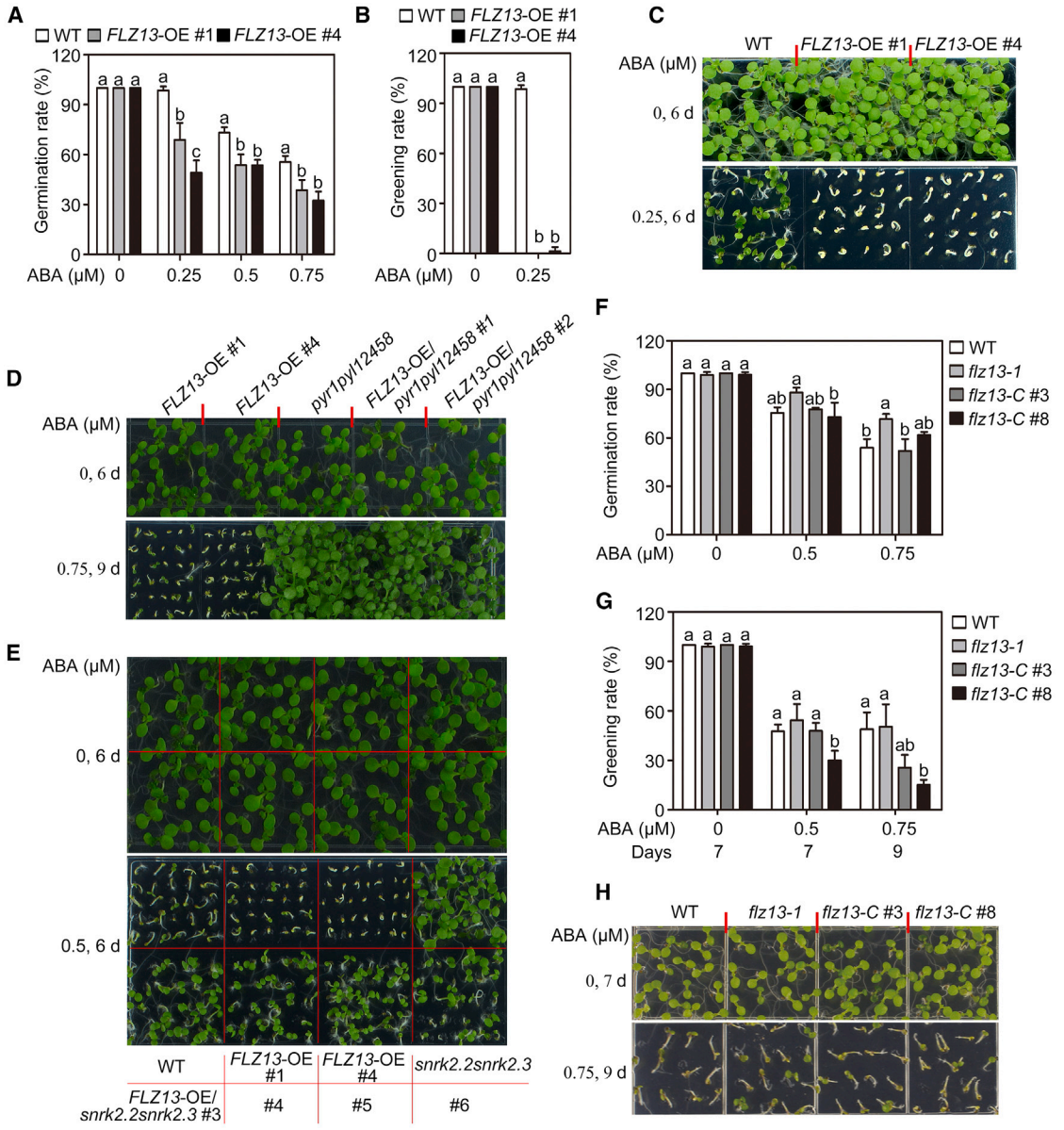

Figure 2. FLZ13 positively regulates ABA response during seed germination.

(A) Germination rates of the WT and *FLZ13*-OE lines. Seed germination rates were recorded 4 days after plating on $^1/_2$ MS medium supplemented with the indicated concentrations of ABA. Data are presented as mean ± SD (n = 3 biological replicates). The different letters above each bar indicate statistically significant differences determined by one-way ANOVA followed by Tukey's multiple comparison test ($P < 0.05$).

(B) Cotyledon greening rates of the WT and *FLZ13*-OE lines. Cotyledon greening rates were scored 6 days after plating on $^1/_2$ MS medium supplemented with 0 or 0.25 μM ABA. Data are presented as mean ± SD (n = 3 biological replicates). The different letters above each bar indicate statistically significant differences determined by one-way ANOVA followed by Tukey's multiple comparison test ($P < 0.05$).

(C) Photographs of seedlings of WT and two *FLZ13*-OE lines germinated on $^1/_2$ MS medium containing 0 or 0.25 μM ABA for 6 days.**(D)** Photographs of seedlings of *FLZ13*-OE, *pyr1pyl12458* (*pyr1pyl1pyl2pyl4pyl5pyl8*), and *FLZ13*-OE/*pyr1pyl12458* lines after 0 μM ABA treatment for 6 days or 0.75 μM ABA treatment for 9 days.**(E)** Photographs of seedlings of WT, *FLZ13*-OE, *snrk2.2snrk2.3*, and *FLZ13*-OE/*snrk2.2snrk2.3* lines after 0 or 0.5 μM ABA treatment for 6 days.**(F)** Germination rates of the WT, *flz13-1*, and two *gFLZ13*/*flz13-1* complementation lines (*flz13*-C #3 and *flz13*-C #8). Seed germination rates were recorded 4 days after plating on $^1/_2$ MS medium supplemented with various concentrations of ABA, as indicated. Data are presented as mean ± SD (n = 3 biological replicates). The different letters above each bar indicate statistically significant differences determined by one-way ANOVA followed by Tukey's multiple comparison test ($P < 0.05$).

(G) Cotyledon greening rates of WT, *flz13-1*, and two *gFLZ13*/*flz13-1* complementation lines (*flz13*-C #3 and *flz13*-C #8) treated with various ABA concentrations as recorded at the indicated time points. Data are presented as mean ± SD (n = 3 biological replicates). The different letters above each bar indicate statistically significant differences determined by one-way ANOVA followed by Tukey's multiple comparison test ($P < 0.05$).

(H) Photographs of seedlings of WT, *flz13-1*, and two *gFLZ13*/*flz13-1* complementation lines (*flz13*-C #3 and *flz13*-C #8) after treatment with 0 μM ABA for 7 days or 0.75 μM ABA for 9 days.

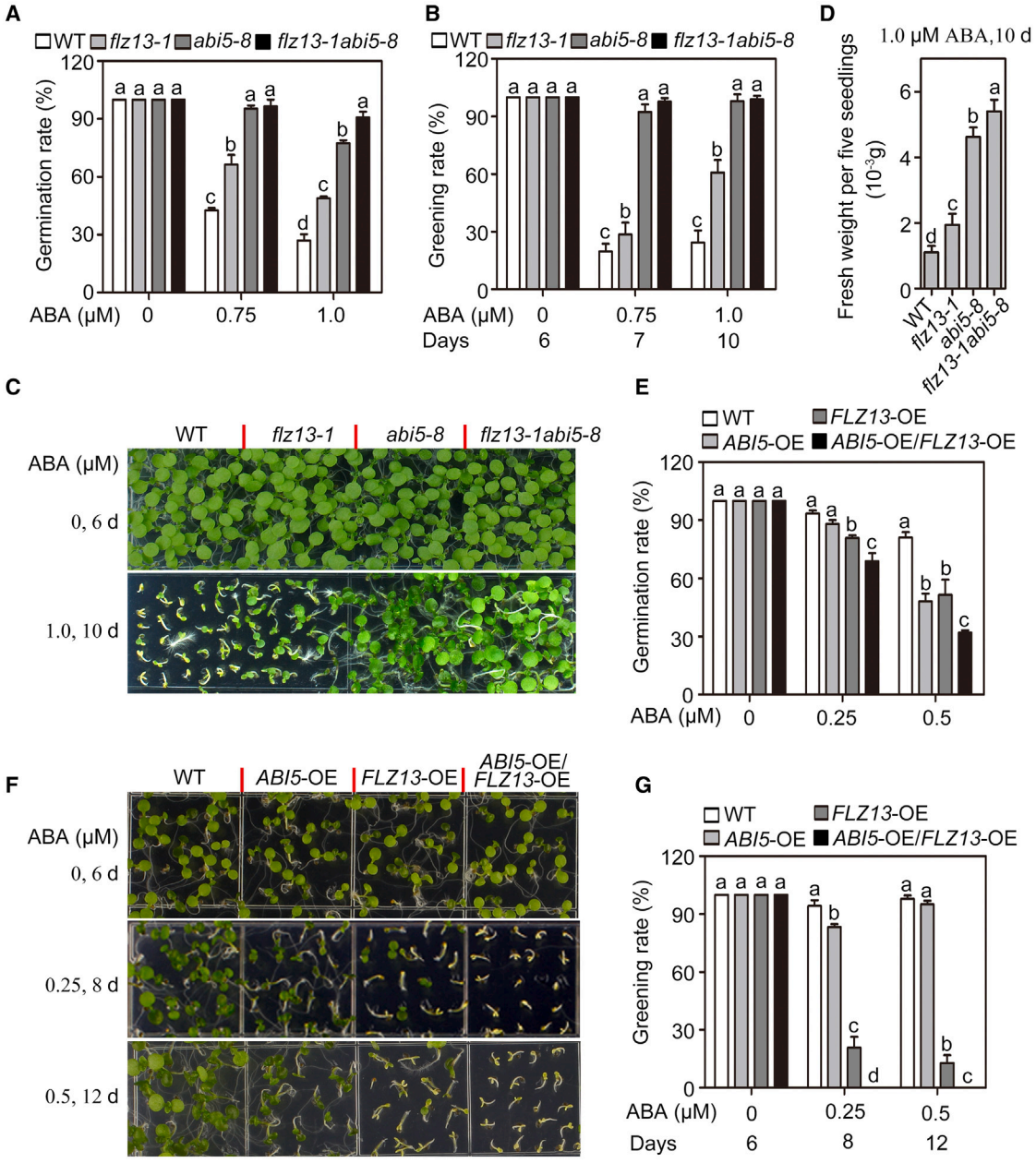

Figure 3. Genetic interaction between FLZ13 and ABI5 in ABA signaling during seed germination.

(A) Germination rates of the WT and *flz13-1*, *abi5-8*, and *flz13-1abi5-8* mutants treated with the indicated concentrations of ABA. Germination rates were recorded 4 days after plating on $^1/_2$ MS medium. Data are presented as mean ± SD (n = 3 biological replicates). The different letters above each bar indicate statistically significant differences determined by one-way ANOVA followed by Tukey's multiple comparison test ($P < 0.05$).

(B) Cotyledon greening rates of WT, *flz13-1*, *abi5-8*, and *flz13-1abi5-8* plants treated with various concentrations of ABA at different time points as indicated. Data are presented as mean ± SD (n = 3 biological replicates). The different letters above each bar indicate statistically significant differences determined by one-way ANOVA followed by Tukey's multiple comparison test ($P < 0.05$).

(C) Photographs of seedlings of WT, *flz13-1*, *abi5-8*, and *flz13-1abi5-8* treated with various concentrations of ABA at different time points, as indicated.

(D) Fresh weight of five seedlings of WT, *flz13-1*, *abi5-8*, and *flz13-1abi5-8* treated with 1.0 μM ABA for 10 days. Data are presented as mean ± SD (n = 5 biological replicates). The different letters above each bar indicate statistically significant differences determined by one-way ANOVA followed by Tukey's multiple comparison test ($P < 0.05$).

(E) Germination rates of WT, *ABI5*-OE, *FLZ13*-OE, and *ABI5*-OE/*FLZ13*-OE plants treated with the indicated concentrations of ABA. Germination rates were recorded 4 days after plating on $^1/_2$ MS medium. Data are presented as mean ± SD (n = 3 biological replicates). The different letters above each bar indicate statistically significant differences determined by one-way ANOVA followed by Tukey's multiple comparison test ($P < 0.05$).

(legend continued on next page)

and 0.75 μM ABA treatment (Figure 2F) but exhibited lower greening rates than the WT and *flz13-1* (Figure 2G and 2H), suggesting that the reduced ABA sensitivity of the *flz13-1* mutant was indeed due to knockdown of *FLZ13*. To obtain additional mutant alleles, CRISPR–Cas9 technology was used to edit *FLZ13* in Col-0 WT plants. We obtained one edited line, *flz13-2*, with a deletion of 16 nucleotides (164–179) predicted to result in a truncated FLZ13 protein (Supplemental Figure 7A). The *flz13-2* mutant showed reduced sensitivity to ABA, as revealed by comparison of the seed germination rate and cotyledon greening rate in the presence of 1.0 μM ABA (Supplemental Figure 7B and 7C). We further tested the responses of the *flz13-1* and *flz13-2* mutants to a relatively high concentration (2.0 μM) of ABA, and the results showed that they were less sensitive to ABA treatment than Col-0 plants, with higher cotyledon greening rates (Supplemental Figure 8). Taken together, these data suggest that *FLZ13* positively regulates ABA signaling to repress seed germination and early seedling growth in *Arabidopsis*.

FLZ13 and ABI5 function additively to modulate ABA signaling

To determine the functional relationship between FLZ13 and ABI5 in ABA signaling, we crossed *flz13-1* with *abi5-8* to generate an *flz13-1abi5-8* double mutant for phenotypic analysis. Consistent with a previous study (Zhou et al., 2015), *abi5-8* seeds germinated and grew much faster than WT seeds on ABA-containing medium (Figure 3A–3D), and *flz13-1* seeds also showed less sensitivity to ABA than WT seeds (Figure 3A–3D). Notably, the *flz13-1abi5-8* double mutant displayed less sensitivity to 1.0 or 2.0 μM ABA treatments compared with the *abi5-8* and *flz13-1* single mutants (Figure 3A–3D and SupplementalFigure 8), suggesting that FLZ13 and ABI5 may function additively to regulate ABA signaling during seed germination. We also crossed our previously established *pUBQ10::ABI5-GFP* #1 line (*ABI5*-OE #1, Li et al., 2019) with *FLZ13*-OE #1 to generate plants that simultaneously overexpressed *ABI5* and *FLZ13* (*ABI5*-OE/*FLZ13*-OE) to test ABA sensitivity. As expected, the progenies of *ABI5*-OE/*FLZ13*-OE displayed significantly lower rates of seed germination and cotyledon greening than those of *ABI5*-OE and *FLZ13*-OE in media with various concentrations of ABA (Figure 3E–3G), further confirming the additive effect of ABI5 and FLZ13 on plant ABA response. Collectively, these data demonstrate that FLZ13 and ABI5 function additively to repress seed germination upon ABA treatment.

FLZ13 and ABI5 regulate common target genes in response to ABA

Observations of the protein and genetic interactions between FLZ13 and ABI5 motivated us to identify genes co-regulated by FLZ13/ABI5 in response to ABA during seed germination. RNA sequencing (RNA-seq) analyses were performed using germinating seeds of WT, *ABI5*-OE #1, and *FLZ13*-OE #1 treated with 0 or 0.5 μM ABA for 3 days. Without ABA treatment, all the seeds of the different genotypes germinated, and the cotyledons were green. With 0.5 μM ABA treatment, approximately 50% of WT seeds germinated, whereas the germination rates of *ABI5*-OE #1 and *FLZ13*-OE #1 seeds were lower than 10%. In WT seeds, 6970 differentially expressed genes (DEGs) (fold change $\geq$2, false discovery rate [FDR] <0.01) were identified (Figure 4A; Supplemental Table 4), including 77 genes previously found to be induced by ABA (Supplemental Table 5), indicating that this batch of RNA-seq data were reliable. Compared with the WT, 1161 and 1181 DEGs were identified in *ABI5*-OE #1 and *FLZ13*-OE #1 seeds with 0.5 μM ABA treatment (Figure 4A; Supplemental Tables 6 and 7).

To identify ABA-responsive genes that were also co-regulated by ABI5 and FLZ13, we selected genes that met the following three criteria: (1) genes were differentially expressed after ABA treatment in the WT; (2) their expression differed between WT and *ABI5*-OE #1 after ABA treatment; and (3) their expression differed between WT and *FLZ13*-OE #1 after ABA treatment. Finally, 567 genes were identified as ABA-responsive and ABI5–FLZ13 co-regulated (Figure 4A; Supplemental Table 8). A heatmap showed that only four genes were upregulated, whereas most genes (496, 87.5%) were simultaneously suppressed by ABA, ABI5, and FLZ13 (Figure 4B), and they all showed induced expression patterns during seed germination (Figure 4C). Gene Ontology (GO) term enrichment analysis revealed that these 496 DEGs were mainly enriched in categories related to growth, including "photosynthesis" (41 genes, P = 3.6E−22) and "cell wall organization" (40 genes, P = 1.7E−11) (Figure 4D; Supplemental Table 9). Furthermore, among the 496 genes, 126 were targeted by ABI5, as verified by chromatin immunoprecipitation sequencing (ChIP-seq) and/or DNA affinity purification sequencing (DAP-seq) assays (O'Malley et al., 2016) (Figure 4E; Supplemental Table 10). The set of 35 high-confidence ABI5-targeted genes, as verified by both ChIP-seq and DAP-seq assays, contained genes encoding 18 photosynthesis-related proteins, six cell wall–modification related proteins, three transcription factors, and two kinases (Figure 4F; Supplemental Table 11). Collectively, these results indicate that FLZ13 and ABI5 display overlapping functions in determining plant responses to ABA by co-targeting a subset of ABA-responsive genes, especially ABA-repressed and growth-related genes.

FLZ13 activation of ABA signaling requires a functional ABI5

To study the genetic epistasis between *FLZ13* and *ABI5*, we explored whether the action of FLZ13 in mediating ABA signaling requires a functional ABI5 by generating plants that overexpressed *FLZ13* in the *abi5-8* mutant background. Progenies of *FLZ13*-OE/*abi5-8* were hyposensitive to 0.5 μM ABA treatment during seed germination, with higher seed germination percentages and cotyledon greening rates than WT and *FLZ13*-OE plants (Figure 5A–5C). However, compared with the *abi5-8* mutant,

(F) Photographs of WT, *ABI5*-OE, *FLZ13*-OE, and *ABI5*-OE/*FLZ13*-OE seedlings germinated on media containing various concentrations of ABA at different time points as indicated.

(G) Cotyledon greening rates of WT, *ABI5*-OE, *FLZ13*-OE, and *ABI5*-OE/*FLZ13*-OE plants treated with various concentrations of ABA at different time points as indicated. Data are presented as mean ± SD (n = 3 biological replicates). The different letters above each bar indicate statistically significant differences determined by one-way ANOVA followed by Tukey's multiple comparison test (P < 0.05).

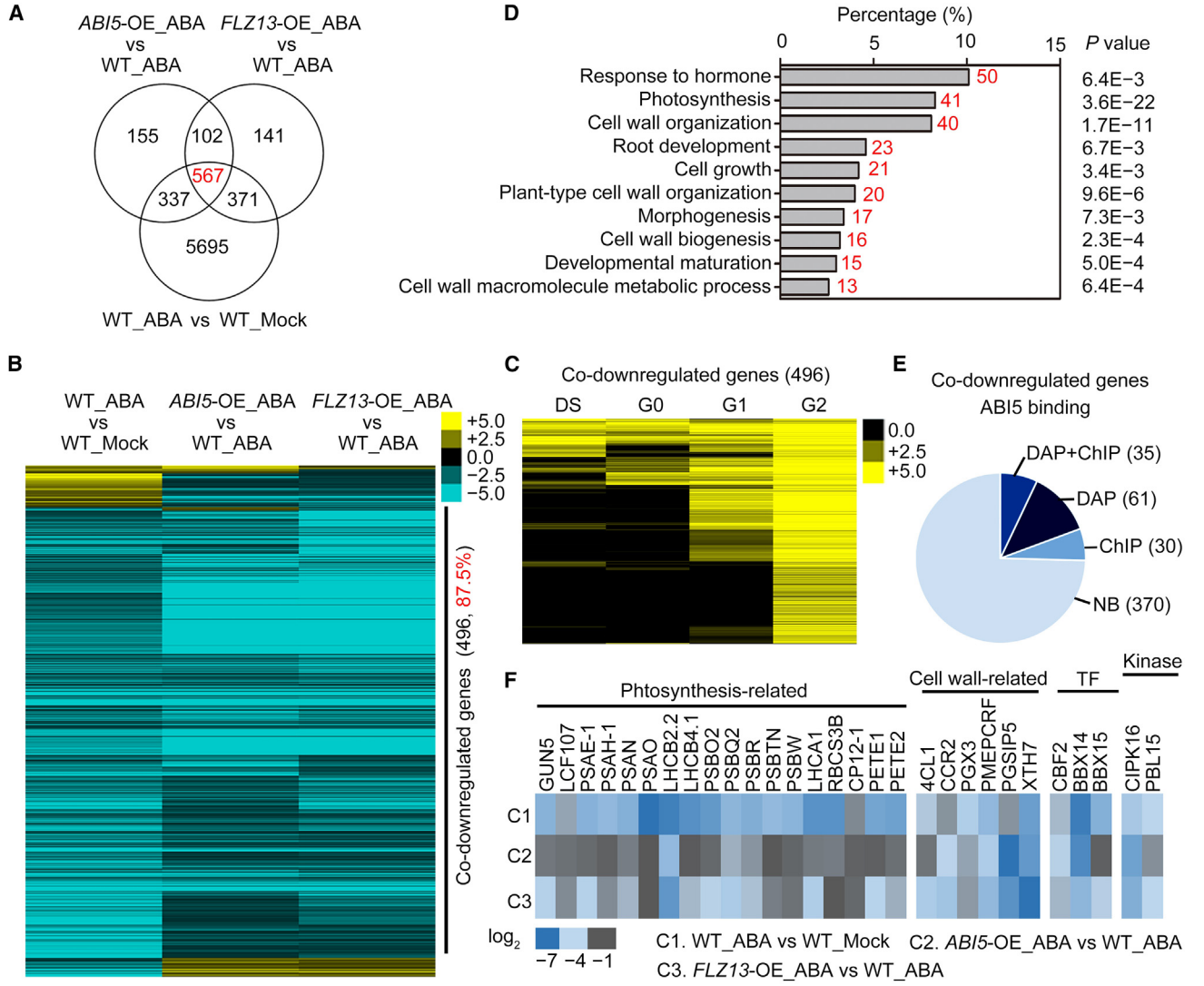

Figure 4. Identification of ABA/ABI5/FLZ13 co-regulated genes.

(A) Venn diagram showing the overlap of ABA/ABI5/FLZ13-regulated genes.

(B) Heatmap showing the expression of ABA/ABI5/FLZ13 co-regulated genes. The expression data were clustered using Cluster 3.0 software and edited in TreeView.

(C) Heatmap showing the expression of ABA/ABI5/FLZ13 co-repressed genes during seed germination. The expression data were obtained from a publicly available database (http://bioinfo.sibs.ac.cn/plant-regulomics/; Ran et al., 2020), clustered with Cluster 3.0 software, and edited in TreeView. DS, dry seed; G0, G1, and G2 indicate germinating seeds at 0, 1, and 2 days, respectively.

(D) Representative enriched BP terms of the ABA/ABI5/FLZ13 co-repressed genes. GO enrichment analysis was performed using an online program (https://david.ncifcrf.gov; Huang et al., 2009). Red numbers indicate gene numbers.

(E) Pie chart showing the number of ABA/ABI5/FLZ13 co-repressed genes bound by ABI5 in ChIP-seq and/or DAP-seq assays (O'Malley et al., 2016). NB, not bound.

(F) Heatmap showing the expression of well-annotated ABI5 target genes that are co-repressed by ABA/ABI5/FLZ13.

FLZ13-OE/*abi5-8* was slightly more sensitive to 0.75 μM ABA, indicating that ABA hypersensitivity conferred by *FLZ13* overexpression was largely but not fully dependent on ABI5 (Figure 5A–5C).

To assess the effect of ABI5 on the expression of *FLZ13*-regulated genes, we carried out RNA-seq analysis using 3-day-old germinating *FLZ13*-OE/*abi5-8* seeds treated with 0.5 μM ABA (Supplemental Table 12). A heatmap of 500 ABA/ABI5/FLZ13 synchronously co-regulated genes showed altered expression patterns. Two-hundred and ninety-seven out of these 500 genes (59.4%) exhibited significant alterations in *FLZ13*-OE/*abi5-8* (Figure 5D, left panel), supporting the notion that FLZ13-mediated transcriptional regulation largely depends on the function of ABI5. For example, 30 of the 35 ABI5 target genes showed differential expression between *FLZ13*-OE/*abi5-8* and *FLZ13*-OE plants after ABA treatment (Figure 5D, right panel). We also performed qRT–PCR to confirm the transcript levels of five ABI5 target genes (*GUN5*, *PSAH1*, *PSBR*, *PSBQ2*, and *XTH7*) (Supplemental Figure 9). The results revealed that

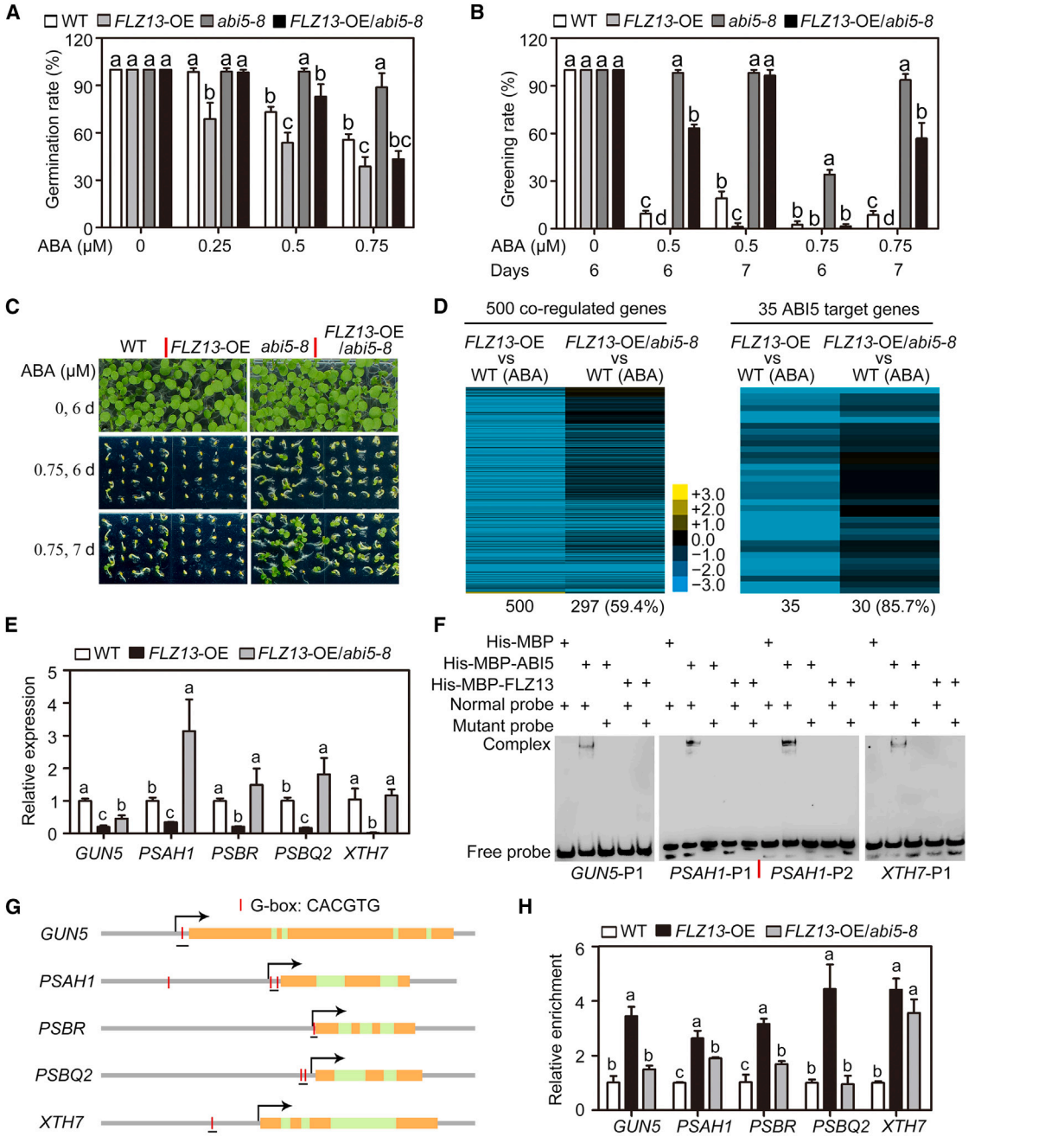

Figure 5. FLZ13 regulates ABA response during seed germination in an ABI5-dependent manner.

(A) Germination rates of WT, *FLZ13*-OE, *abi5-8*, and *FLZ13*-OE/*abi5-8* treated with the indicated concentrations of ABA. Germination rates were recorded 4 days after plating on $^1/_2$ MS medium. Data are presented as mean ± SD (n = 3 biological replicates). The different letters above each bar indicate statistically significant differences determined by one-way ANOVA followed by Tukey's multiple comparison test ($P < 0.05$).

(B) Cotyledon greening rates of WT, *FLZ13*-OE, *abi5-8*, and *FLZ13*-OE/*abi5-8* treated with various concentrations of ABA at different time points, as indicated. Data are presented as mean ± SD (n = 3 biological replicates). The different letters above each bar indicate statistically significant differences determined by one-way ANOVA followed by Tukey's multiple comparison test ($P < 0.05$).

(C) Photographs of WT, *FLZ13*-OE, *abi5-8*, and *FLZ13*-OE/*abi5-8* seedlings germinated on medium containing various concentrations of ABA for the indicated time periods.

(D) Heatmap showing the expression of genes synchronously co-regulated by ABA/ABI5/FLZ13 in *FLZ13*-OE and *FLZ13*-OE/*abi5-8* lines in the presence of ABA. Three-day-old germinating seeds with 0.5 μM ABA treatment were collected for the RNA-seq assay.

(E) Quantitative RT–PCR assay showing expression of the selected genes in WT, *FLZ13*-OE, and *FLZ13*-OE/*abi5-8* upon ABA treatment. Three-day-old germinating seeds with 0.5 μM ABA treatment were collected for the qRT–PCR assay. *PP2A* was used as an internal control. Data are presented as mean ± SD (n = 3 technical replicates). The different letters above each bar indicate statistically significant differences determined by one-way ANOVA followed by Tukey's multiple comparison test ($P < 0.05$). This experiment was repeated twice with similar results.

(legend continued on next page)

mutation of ABI5 largely compromised *FLZ13*-repressed expression of these genes (Figure 5E). The above ABA sensitivity test and gene expression analysis clearly demonstrated that the function of FLZ13 in ABA signaling depends largely on a functional ABI5.

To further explore how ABI5 affects the action of FLZ13, we used an electrophoretic mobility shift assay (EMSA) to examine the DNA-binding ability of ABI5 and FLZ13 to their co-regulated genes. As shown in Figure 5F, ABI5 directly bound to the promoter regions of *GUN5*, *PSAH1*, and *XTH7* via a conserved G-box *cis* element, whereas FLZ13 failed to bind to these regions. To check these bindings *in vivo*, we performed chromatin immunoprecipitation (ChIP) using ABA-treated germinating seeds of *FLZ13*-OE and *FLZ13*-OE/*abi5-8* plants. ChIP–qPCR analysis showed that FLZ13 was enriched at ABI5-bound genomic loci, including *GUN5*, *PSAH1*, *PBSR*, *PBSQ2*, and *XTH7*, in *FLZ13*-OE seeds (Figure 5G and 5H). However, enrichment of FLZ13 on their promoters was generally lower in *FLZ13*-OE/*abi5-8* than in *FLZ13*-OE (Figure 5G and 5H). These findings suggest that FLZ13 is recruited to the promoters of *GUN5*, *PSAH1*, *PBSR*, *PBSQ2*, and *XTH7* at least in part through its interaction with ABI5.

Knockdown of *FLZ13* compromises the function of ABI5

To elucidate the role of FLZ13 in ABI5 activity, we generated an *ABI5*-OE/*flz13-1* plant by crossing and performed an ABA sensitivity test. As shown in Figure 6A and 6B, knockdown of *FLZ13* significantly increased the cotyledon greening rate of *ABI5*-OE plants in the presence of 0.5 μM ABA, suggesting that FLZ13 contributes to the ABI5-modulated ABA response. To explore how FLZ13 functions in the ABI5-mediated ABA response, we analyzed whether FLZ13 affects ABI5 protein stability and phosphorylation, two decisive factors that contribute to ABI5 activity during ABA signaling (Yu et al., 2015). We first examined endogenous ABI5 protein levels in 3-day-old germinating seeds of the WT, *flz13-1*, and *flz13-2* lines with 0 or 0.5 μM ABA treatment. ABI5 was too low to be detected in all the genotypes without ABA treatment but could be detected in these seeds with 0.5 μM ABA treatment, although no obvious differences in ABI5 protein levels were observed among the genotypes (Figure 6C). We then compared ABI5-GFP protein expression in *ABI5*-OE and *ABI5*-OE/*flz13-1* plants. Immunoblotting results demonstrated that the abundance of ABI5-GFP protein was similar in *flz13-1* and WT backgrounds under both normal growth conditions and ABA treatment (Figure 6D), further suggesting that FLZ13 does not regulate the stability of ABI5. Moreover, the phosphorylation levels of immunoprecipitated ABI5-GFP from ABA-treated samples were similar in *flz13-1* and WT backgrounds (Figure 6E), suggesting that FLZ13 did not affect the phosphorylation of ABI5 in response to ABA.

We next analyzed the expression of 500 genes synchronously co-regulated by ABA/ABI5/FLZ13 in 3-day-old germinating seeds of *ABI5*-OE/*flz13-1* upon 0.5 μM ABA treatment using an RNA-seq assay (Supplemental Table 13). A heatmap showed significantly altered expression levels of 181 genes (36.2%) (Figure 6F, left panel), indicating that ABI5-mediated transcriptional regulation of these genes was affected by FLZ13. For instance, 23 of 35 ABI5 target genes showed differential expression between *ABI5*-OE/*flz13-1* and *ABI5*-OE plants treated with ABA (Figure 6F, right panel). We also performed qRT–PCR to confirm the transcript levels of *GUN5*, *PSAH1*, *PBSR*, *PBSQ2*, and *XTH7* and found that mutations in *FLZ13* largely compromised the ABI5-repressed expression of these genes (Figure 6G). Based on these results, we speculated that FLZ13 may affect the DNA-binding ability of ABI5 to its downstream genes. To test this possibility, we performed ChIP–qPCR analysis using ABA-treated germinating seeds of *ABI5*-OE and *ABI5*-OE/*flz13-1*. Enrichment of ABI5 on the promoters of *GUN5*, *PSAH1*, *PBSR*, *PBSQ2*, and *XTH7* was generally lower in *ABI5*-OE/*flz13-1* than in *ABI5*-OE (Figure 6H), indicating that *FLZ13* knockdown decreased the binding of ABI5 to its target genes *in planta*.

DISCUSSION

ABA modulates plant growth or stress responses by triggering massive transcriptional reprogramming that depends mainly on several ABA-responsive transcription factors. In particular, ABI5 functions as the master regulator during ABA-inhibited seed germination and seedling establishment (Chen et al., 2020). However, how *ABI5* modulates ABA-repressed seed germination and seedling establishment remains largely unknown because only a few target genes of ABI5 are directly associated with these processes (Lee and Luan, 2012; Skubacz et al., 2016). Furthermore, the precise regulatory mechanism of the ABI5-engaged transcriptional regulation machinery also remains to be fully clarified.

In this study, we used TurboID-mediated proximity labeling to obtain the ABI5 interactome and identified FLZ13 as a new protein that interacts with ABI5 (Figure 1). FLZs are plant-specific regulatory proteins, and the *Arabidopsis* genome contains 19 FLZ proteins (Jamsheer and Laxmi, 2015). The first FLZ protein, MEDIATOR OF ABA-REGULATED DORMANCY 1 (MARD1/FLZ19), was identified from senescence-related enhancer trapping and has been implicated in ABA-mediated seed germination in *Arabidopsis* (He et al., 2001; He and Gan, 2004). Expression of *MARD1* was induced by ABA treatment, and the seeds of *mard1* were relatively resistant to external ABA during germination (He and Gan, 2004). Recently, *FLZ6*, *FLZ8*, and *FLZ10* were also reported to participate in plant ABA responses by interfering with SUCROSE NON-FERMENTING1 (SNF1)-RELATED KINASE 1 (SnRK1) and TARGET OF RAPAMYCIN (TOR) signaling (Jamsheer et al., 2018, 2022). In an ABA-inhibited root elongation assay, *flz6.1* and *flz10.1* showed slightly higher

(F) EMSA showing the binding ability of ABI5 and FLZ13 to the ABI5 target genes *GUN5*, *PSAH1*, and *XTH7*. The DNA probes used in this experiment are shown in Supplemental Figure 9. In the mutant probes, the G-box sequence (CACGTG) was replaced with CTTTTG. The probe sequences are listed in Supplemental Table 14.

(G) Structure of selected ABI5 target genes. The positions of the G-box and fragments used for the ChIP–PCR assay are marked.

(H) ChIP–qPCR assay showing the relative enrichment of FLZ13 at the selected gene locus. Data are presented as mean ± SD ($n = 3$ technical replicates). The different letters above each bar indicate statistically significant differences determined by one-way ANOVA followed by Tukey's multiple comparison test ($P < 0.05$). This experiment was repeated twice with similar results.

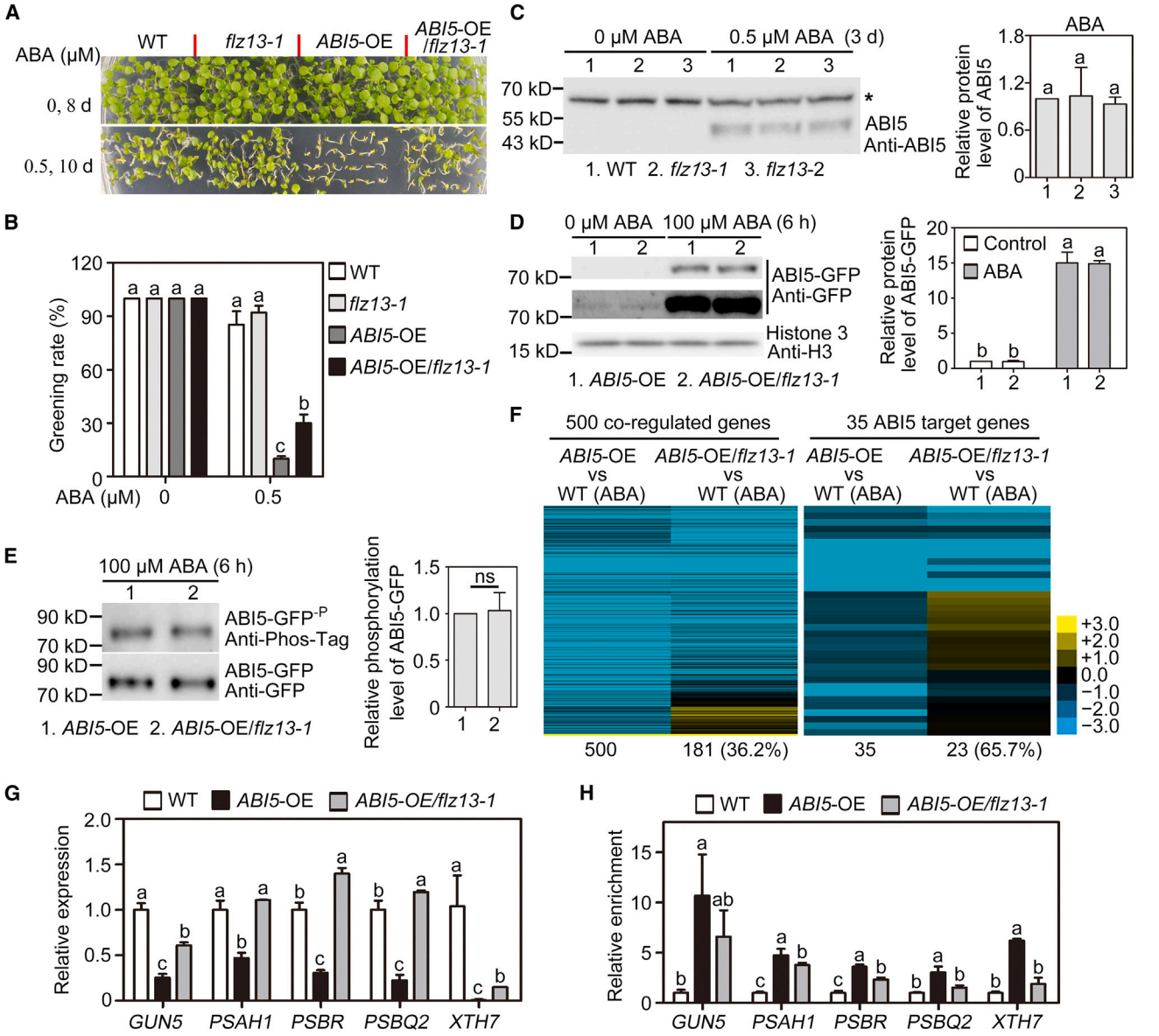

Figure 6. The function of ABI5 during seed germination is partially compromised in *FLZ13* mutants.

(A) Photographs of WT, *flz13-1*, *ABI5*-OE, and *ABI5*-OE/*flz13-1* seedlings germinated on media containing various concentrations of ABA for the indicated time periods.

(B) Cotyledon greening rates of WT, *flz13-1*, *ABI5*-OE, and *ABI5*-OE/*flz13-1* plants upon treatment with various concentrations of ABA at the indicated time points. Data are presented as mean ± SD ($n = 3$ biological replicates). The different letters above each bar indicate statistically significant differences determined by one-way ANOVA followed by Tukey's multiple comparison test ($P < 0.05$).

(C) Immunoblotting analysis of ABI5 protein in the WT and *flz13* mutants. Three-day-old germinating seeds sown on $^1/_2$ MS plates with 0 or 0.5 μM ABA treatment were harvested for protein extraction and western blot analysis using anti-ABI5 antibodies. The relative protein levels of ABI5 in ABA-treated samples are shown on the left. Data are presented as mean ± SD ($n = 4$ biological replicates). An asterisk (*) indicates non-specific bands that were used as loading controls. The different letters above each bar indicate statistically significant differences determined by one-way ANOVA followed by Tukey's multiple comparison test ($P < 0.05$).

(D) Immunoblotting analysis of ABI5-GFP protein in the WT and *flz13-1* backgrounds. Whole seedlings of 7-day-old *ABI5*-OE and *ABI5*-OE/*flz13-1* were treated with 0 (Control) or 100 μM ABA for 6 h before protein extraction for western blot analysis using anti-GFP and anti-H3 antibodies. Short (upper panel) and long (middle panel) exposures of blots for ABI5-GFP are shown. The protein levels of ABI5-GFP relative to that of histone 3 are shown on the left. Data are presented as mean ± SD ($n = 3$ biological replicates). The different letters above each bar indicate statistically significant differences determined by one-way ANOVA followed by Tukey's multiple comparison test ($P < 0.05$).

(E) Phosphorylation of ABI5-GFP protein in the WT and *flz13-1* background upon ABA treatment. Whole seedlings of 7-day-old *ABI5*-OE and *ABI5*-OE/*flz13-1* plants were treated with 100 μM ABA for 6 h before protein extraction for immunoprecipitation using GFP-Trap beads. The samples were then subjected to western blot analysis using anti-GFP and anti-Phos-tag antibodies. Relative phosphorylation levels of ABI5-GFP are shown on the left. Data are presented as mean ± SD ($n = 3$ biological replicates). Statistical analysis was performed using Student's *t*-test. ns, no significant difference.

(legend continued on next page)

sensitivity to external ABA, whereas *flz8.1* showed lower sensitivity (Jamsheer et al., 2018, 2022). Here, we offer several lines of evidence to show that FLZ13 positively regulates the ABA response during the embryo-to-seedling transition. First, FLZ13 directly interacts with ABI5, a core transcription factor in ABA signaling (Skubacz et al., 2016), and this interaction is responsive to ABA treatment (Figure 1 and SupplementalFigure 4). Second, progenies of the *flz13* mutant were less sensitive to ABA, whereas those of *FLZ13*-overexpressing plants were much more sensitive to ABA than WT plants during seed germination and seedling establishment (Figures 2 and 3 and SupplementalFigures 7 and 8). Third, FLZ13 and ABI5 co-regulate a large subset of genes in response to ABA (Figure 4). Finally, FLZ13 and ABI5 function interdependently to mediate the ABA response during seed germination and seedling establishment (Figures 5 and 6). These results strongly suggest that FLZ13 works together with ABI5 to positively regulate ABA signaling during seed germination. We also verified that ABA receptors and subclass III SnRK2s are required for *FLZ13* to positively regulate ABA signaling (Figure 2D and 2E). However, it is worth noting that the phenotypes of *flz13* mutants were much weaker than those of *abi5-8* in response to ABA treatment (Figure 3A and 3B and SupplementalFigure 8). In the *Arabidopsis* genome, *FLZ13* has two close homologs (*FLZ12* and *FLZ14*) (Jamsheer and Laxmi, 2015), which raises the possibility that *FLZ13* may function redundantly with *FLZ12* and *FLZ14* to regulate ABA responses, although the detailed biological roles of *FLZ12* and *FLZ14* remain to be determined.

The *flz13-1abi5-8* double mutant exhibited higher germination and greening percentages than *flz13-1* and *abi5-8* single mutants in the presence of ABA, and *FLZ13*-OE/*ABI5*-OE showed higher sensitivity to ABA than *FLZ13*-OE and *ABI5*-OE (Figure 3), indicating that ABI5 and FLZ13 have additive effects on the promotion of ABA response during seed germination. As shown in Figure 4A, transcriptome analyses identified 567, 337, and 371 ABA-responsive genes that were co-regulated or specifically regulated by ABI5 and FLZ13, respectively, implying that FLZ13 and ABI5 can also function with other modulators to regulate different gene sets to determine ABA signaling. For example, PRR5 and PRR7 can interact with ABI5 to enhance its function in ABA signaling and inhibit seed germination in the presence of ABA (Yang et al., 2021). Although we failed to observe an interaction between FLZ13 and other critical transcription factors of ABA signaling such as ABI3, ABI4, ABF2, and ABF4 (Supplemental Figure 3) in the Y2H assay, we cannot exclude the possibility that FLZ13 associates with other modulators to affect their activity in ABA signaling. For instance, a recent study showed that ZmFLZ25 interacts with several ABA receptors to confer hypersensitivity to ABA during seed germination (Chen et al., 2021).

Interestingly, the ABA sensitivity of the *ABI5*-OE/*flz13-1* progenies was between that of *flz13-1* and *ABI5*-OE plants (Figure 6A and 6B), indicating that the action of ABI5 during ABA signaling is partially dependent on FLZ13. FLZ13 did not affect the protein stability or phosphorylation of ABI5 in the presence of ABA (Figure 6C–6E), but it was partially required for the DNA binding of ABI5 to downstream target genes (Figure 6H). The bZIP domain associated with ABI5 dimerization and DNA binding (Finkelstein and Lynch, 2000) was involved in the interaction with FLZ13 (Figure 1D), and FLZ13 is an FCS-like zinc-finger protein that can be recruited to *GUN5*, *PBSR*, *PSAH1*, *PBSQ2*, and *XTH7* promoters through interaction with ABI5 (Figure 5H). It is therefore possible that the FLZ13–ABI5 complex functions similarly to the ABI5 dimer and shows increased binding activity to promoters of target genes. Future studies need to be performed to explore the detailed biochemical mechanisms by which FLZ13 synergizes with ABI5 to modulate downstream genes.

RNA-seq analysis identified 567 genes co-regulated by ABA, ABI5, and FLZ13 (Figure 4A; Supplemental Table 8). Interestingly, most of the FLZ13 and ABI5 co-regulated genes were repressed by ABA (Figure 4B), suggesting that ABI5 and FLZ13 play important roles in ABA-mediated transcriptional repression. Interestingly, these co-repressed genes were mainly enriched in categories related to growth, including "photosynthesis" (41 genes, $P = 3.6E-22$) and "cell wall organization" (40 genes, $P = 1.7E-11$) (Figure 4D; Supplemental Table 9). However, ABI5 is a transcription factor with strong transcriptional activation activity, and how the ABI5–FLZ13 complex represses target gene expression remains unclear. It is possible that the ABI5–FLZ13 complex recruits transcriptional corepressors to target gene loci and modulates their expression. For example, the mediator (a bridge between transcription factors and RNA polymerase II during transcription) subunit MED16 interacts with ABI5 to repress the expression of ABI5 target genes (Guo et al., 2021). In our ABI5-interactome data, several transcriptional corepressors, such as LEUNIG, SUESS, and TETRATRICOPEPTIDE REPEAT 2 (TPR2) (Franks et al., 2002; Long et al., 2006), showed significantly higher enrichment in the ABI5-TurboID-GFP vs. TurboID-GFP pairs (Supplemental Table 1). They were positioned at the central nodes of the PPI networks (Supplemental Figure 2), indicating their important roles in ABI5-mediated transcriptional repression. Further investigation of the underlying molecular mechanisms will provide new insights into the genetic basis of ABI5–FLZ13-inhibited seed germination and post-germination growth.

(F) Heatmap showing the expression of genes synchronously co-regulated by ABA/ABI5/FLZ13 in *ABI5*-OE and *ABI5*-OE/*flz13-1* lines in the presence of ABA. Three-day-old germinating seeds with 0.5 μM ABA treatment were collected for the RNA-seq assay.
(G) Quantitative RT–PCR assay showing the expression of selected genes in WT, *ABI5*-OE, and *ABI5*-OE/*flz13-1* upon ABA treatment. Three-day-old germinating seeds with 0.5 μM ABA treatment were collected for the qRT–PCR assay. *PP2A* was used as an internal control. Data are presented as mean ± SD ($n = 3$ technical replicates). The different letters above each bar indicate statistically significant differences determined by one-way ANOVA followed by Tukey's multiple comparison test ($P < 0.05$). This experiment was repeated twice with similar results.
(H) ChIP–qPCR assay showing the relative enrichment of ABI5 at the selected gene locus. Data are presented as mean ± SD ($n = 3$ technical replicates). The different letters above each bar indicate statistically significant differences determined by one-way ANOVA followed by Tukey's multiple comparison test ($P < 0.05$). This experiment was repeated twice with similar results.

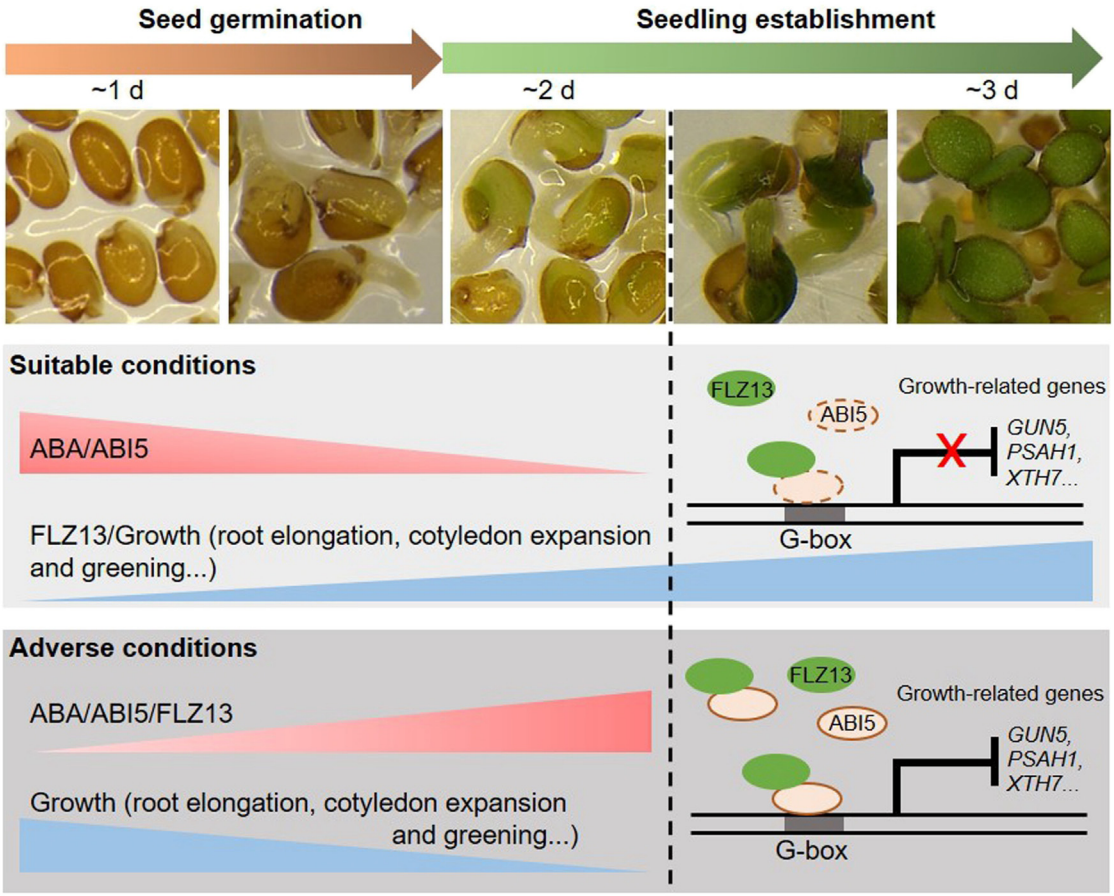

Figure 7. A working model for the ABI5–FLZ13 module in seed germination and seedling establishment.
After seed germination under suitable conditions, the level of ABA and the activity of ABI5 decrease, diminishing the suppression of downstream growth-related genes to promote normal germination and seedling establishment. If germinating seeds are exposed to adverse conditions, the increased ABA activates ABI5, and the ABI5–FLZ13 module represses transcription of growth-related genes to arrest seedling establishment.

In summary, our study sheds new light on how ABI5-mediated ABA signaling represses seed germination and seedling establishment (Figure 7). After seed germination under suitable conditions, ABA levels and ABI5 activity decrease, resulting in diminished suppression of downstream growth-related genes to ensure normal germination and seedling establishment. If adverse conditions are imposed on germinating seeds, elevated ABA activates ABI5, and the ABI5–FLZ13 module represses transcription of growth-related genes to arrest seedling establishment until suitable conditions appear. These findings might be helpful in resetting the balance between growth and stress resistance based on the ABA pathway, thus enabling the engineering of stress-resistant and high-yielding crops in the future.

METHODS

Plant materials and growth conditions

All *Arabidopsis* (*Arabidopsis thaliana*) lines used in this study were in the Col-0 background. The *abi5-8* mutant and *ABI5* overexpression plants (*pUBQ10::ABI5-GFP*, *ABI5*-OE #1) were used as described previously (Zhou et al., 2015; Li et al., 2019). The *flz13-1* mutant (SALK_142112C) was obtained from the ABRC (https://abrc.osu.edu/). The *FLZ13*-Cas9 line (*flz13-2*) was generated using the CRISPR–Cas9 system with two guide RNA sequences (Xing et al., 2014). To generate *FLZ13*-OE transgenic lines, full-length *FLZ13* was cloned in-frame into the binary vector pCAMBIA1300 fused with *GFP* at the C terminus under the control of the *Arabidopsis UBQ10* promoter. The resulting construct was introduced into Col-0, *pyr1pyl1pyl2pyl4pyl5pyl8* (*pyr1pyl12458*) (Gonzalez-Guzman et al., 2012), and *snrk2.2snrk2.3* (Fujii et al., 2007) by *Agrobacterium*-mediated transformation using the floral dip method (Clough and Bent, 1998). To generate *pFLZ13::FLZ13-GFP* plants, the entire genomic sequence of *FLZ13* containing a ~2.0-kb promoter sequence was PCR amplified and inserted into the binary vector pCAMBIA1300 and fused in-frame with *GFP* at the C terminus. The resulting construct was introduced into Col-0 via *Agrobacterium*-mediated transformation using the floral dip method. To generate *gFLZ13/flz13-1* (*flz13-C*) lines, the entire genomic sequence of *FLZ13* containing a ~2.0-kb promoter sequence and a ~1.0-kb terminator sequence was PCR amplified and inserted into the binary vector pCAMBIA1300. The resulting construct was introduced into *flz13-1* via *Agrobacterium*-mediated transformation using the floral dip method. Full-length *TurboID* was cloned into pCAMBIA1300 and fused in-frame with *GFP* at the C terminus under the control of the *Arabidopsis UBQ10* promoter to generate the TurboID-GFP construct. To generate *ABI5-TurboID-GFP*, full-length *ABI5* was inserted

into TurboID-GFP to fuse it with TurboID-GFP at the C terminus. The resulting constructs were introduced into Col-0 via *Agrobacterium*-mediated transformation using the floral dip method. T_0 seeds were screened in ½ Murashige and Skoog (MS) medium containing hygromycin (25 mg/ml). Homozygous plants from the T_3 generation were used in subsequent studies. The *flz13-1abi5-8*, *FLZ13*-OE/*abi5-8*, and *ABI5*-OE/*flz13*-1 plants were generated by crossing and genotyping. The primers used are listed in Supplemental Table 14.

Seeds were surface sterilized with 30% (v/v) bleach for 5 min, washed with double-distilled H_{2O} three times (3 min each time), kept at 4°C in the dark for 2–3 days, and then sown on ½ MS plates supplemented with 0.8% (w/v) agar and 1% sucrose. After 6 days, the well-established seedlings were transferred to soil and grown in a growth chamber at 22°C under long-day conditions (LD, 16 h light/8 h dark). *Nicotiana benthamiana* plants were grown in the same chambers under LD conditions for BiFC and LCI assays.

ABA sensitivity test

Germination and greening of seeds from different genotypes were determined as previously described (Li et al., 2019). In brief, seeds were surface sterilized and then cold stratified at 4°C in the dark for 2–3 days before being sown on ½ MS medium plates with or without various concentrations of ABA (Sangon Biotech, E813BA0006). The plates were placed in a growth chamber at 22°C under LD conditions for germination. After 3–4 days, germination was determined from the appearance of the embryonic axis (appearance of radicle protrusion) as observed under a microscope. After 6–12 days, pictures were taken to calculate the greening rate (appearance of green cotyledons on seedlings) using Adobe Photoshop software. These experiments were performed at least three times with similar results, and around 50–100 seeds of each genotype were used for each biological replicate.

Proximity labeling, affinity purification, and mass spectrometry

Five-day-old *TurboID-GFP* and *ABI5-TurboID-GFP* transgenic seedlings grown on plates with ½ MS medium were transferred to ½ MS liquid medium supplemented with 100 μM ABA for 4 h. This was followed by incubation with 50 μM biotin for 1 h. Then, the seedlings were rinsed with ice-cold water three times for 5 min each to stop the labeling reaction. The seedlings were blotted dry with paper towels and separated into aliquots of approximately 0.6 g fresh weight for the three biological replicates, then stored at −80°C until use.

Total proteins were extracted from the samples with 6 ml of buffer (50 mM Tris [pH 7.5], 150 mM NaCl, 0.1% SDS, 1 mM EDTA, 1% Triton X-100, 0.5% Na-deoxycholate, 1 mM DTT, 1× complete protease inhibitor cocktail, and 1 mM PMSF). Before affinity purification with streptavidin-coated magnetic beads (MedChemExpress, HY-K0208), the protein extract was desalted to remove free biotin using Zeba Spin Desalting Columns (Thermo Fisher, 89893) according to the manufacturer's instructions. Affinity purification was performed at 4°C for approximately 16 h. After affinity purification, the beads were washed five times with the extraction buffer. The samples were then digested on beads with trypsin and analyzed by liquid chromatography–tandem mass spectrometry following established protocols (Branon et al., 2018; Mair et al., 2019).

Proteomic analysis and PPI network construction

Detailed proteomic analysis was performed as described previously (Mair et al., 2019). Filtering and statistical analyses were performed using Perseus (Tyanova et al., 2016). The output file from MaxQuant was imported into Perseus, using label-free quantitation (LFQ) intensities as the main category. The data matrix was filtered to remove proteins marked as "only identified by site," "reverse," and "potential contaminants." LFQ values were $\log_2$ transformed, and proteins that were identified in only one of three replicates of a single genotype were removed. The criteria for identification of ABI5-specific substrates were fold change (ABI5-TurboID-GFP vs. TurboID-GFP) >2 and P value <0.05. Finally, a volplot was generated using the OmicShare tools platform (http://www.omicshare.com/tools), and PPI networks were constructed online (https://metascape.org/; Zhou et al., 2019).

Protein interaction analysis

(1) Yeast two-hybrid (Y2H) assay. Full-length and truncated versions of *FLZ13* or other tested proteins were cloned into pGBKT7 to generate bait vectors with the Gal4 DNA-binding domain. The primers used are listed in Supplemental Table 14. Full-length and truncated versions of *ABI5* were cloned into pGADT7 to generate prey vectors with the Gal4 activation domain, as described previously (Li et al., 2019). The Y2H assay was performed as described previously (Yang et al., 2018). The bait and prey vectors were co-transformed into the yeast strain AH109, and physical interactions were determined by the growth of co-transfected yeast cells on synthetic dropout medium (SD)-Leu-Trp or SD-Leu-Trp-His-adenine plates for 3–4 days after plating.

(2) BiFC. Full-length coding sequences of *FLZ13* and *ABI5* were cloned into the pCAMBIA1300-YN or pCAMBIA1300-YC vector to generate FLZ13-YN and ABI5-YC, respectively. The primers used are listed in Supplemental Table 14. The resulting constructs were transformed into *Agrobacterium tumefaciens* strain GV3101. *A. tumefaciens* containing FLZ13-YN, *A. tumefaciens* containing ABI5-YC, and *A. tumefaciens* containing Histone3-mCherry were co-injected into fully expanded leaves of 4-week-old *N. benthamian* plants at a ratio of 2:2:1. After infiltration for 3 days, the infiltrated regions were observed and imaged using a confocal microscope.

(3) LCI assays. Full-length coding sequences of *FLZ13* and *ABI5* were cloned into the pCAMBIA1300-nLUC and pCAMBIA1300-cLUC vectors to generate FLZ13-nLUC and cLUC-ABI5, respectively. The primers used are listed in Supplemental Table 14. The resulting constructs were transformed into *A. tumefaciens* strain GV3101. *A. tumefaciens* containing FLZ13-nLUC, *A. tumefaciens* containing cLUC-ABI5, and *A. tumefaciens* containing P19 were co-injected into fully expanded leaves of 4-week-old *N. benthamiana* plants at a ratio of 2:2:1. After infiltration for 40 hours, the infiltrated regions were injected with 1 mM luciferin before capturing LUC activity with a Tanon 5200 imaging system. For ABA treatment, leaves were pre-treated with 10 μM ABA for 4 h.

(4) Pull-down assay. Full-length *FLZ13* and *ABI5* were cloned into pMAL-c2× and pGEX4T-3 plasmids, respectively. The primers used are listed in Supplementary Table 14. The recombinant vectors were transformed into *Escherichia coli* BL21 (DE3) to express His-MBP-FLZ13 and GST-ABI5 proteins at 25°C for 6 h with 0.4 mM IPTG induction. The supernatant containing His-MBP or His-MBP-FLZ13 proteins was mixed with 50 μl of MBP-magic beads (Sangon) and incubated for 2 h at 4°C. The beads were then washed six times with 1 ml of PBS and incubated with the supernatant containing GST-ABI5 protein for 4 h at 4°C. After six washes with 1 ml of PBS, the beads were boiled in 30 μl of 1× SDS–PAGE loading buffer. Finally, the presence of GST- and MBP-tagged proteins was detected by western blotting using anti-GST and anti-MBP antibodies.

Gene expression analysis by qRT–PCR

To analyze *FLZ13* and *ABI5* expression during seed germination and its response to ABA, 50 mg of Col-0 seeds were surface sterilized and then cold stratified at 4°C in the dark for 3 days before being sown on ½ MS medium plates with or without 0.5 μM ABA. The plates were placed in a growth chamber at 22°C under LD conditions for germination, and the seeds were harvested at the indicated time points for total RNA isolation using a HiPure Plant RNA Mini Kit (Magen). Total RNA (1 μg) was reverse transcribed using HiScript II Q Select RT SuperMix (Vazyme), and the resulting first-strand cDNA was used as a template for quantitative real-time PCR performed on a CFX96 Touch Real-Time PCR Detection System (Bio-Rad) with iTaq Universal SYBR Green Supermix (Bio-Rad). The expression of *PP2A* or *Actin2* was used as an internal control, and relative expression was calculated using the $2^{-\Delta\Delta Ct}$ method. The primer pairs used for the qRT–PCR assay are listed in Supplemental Table 14.

RNA-seq and data analyses

To perform RNA-seq analysis, 200 mg of seeds were surface sterilized and then cold stratified at 4°C in the dark for 3 days before being sown on ½ MS medium plates with or without 0.5 μM ABA. The plates were placed in a growth chamber at 22°C under LD conditions for germination. After 3 days, the seeds were harvested for total RNA isolation using a HiPure Plant RNA Mini Kit (Magen). RNA-seq was performed by Biomarker Technologies. Genes with a $\log_2$ (fold change) ≥ 1 and an average reads per kilobase of transcript per million reads mapped (RPKM) value from three biological repeats >1.0 in at least in one pair were identified as reliable DEGs. Multiple testing was corrected via FDR estimation, and an FDR <0.01 was considered to indicate differential expression. The transcriptome data have been deposited in the Genome Sequence Archive at the National Genomics Data Center, China National Center for Bioinformation/Beijing Institute of Genomics, Chinese Academy of Sciences (https://ngdc.cncb.ac.cn/gsa, CRA011240) and the NCBI GEO repository (http://www.ncbi.nlm.nih.gov/geo, PRJNA885244). GO enrichment analysis was performed using DAVID (https://david.ncifcrf.gov) (Huang et al., 2009). Heatmaps were generated using Cluster 3 software and visualized using TreeView.

ChIP–qPCR assay

ChIP assays were performed as described previously (Gendrel et al., 2005; Yang et al., 2020). In brief, 3-day-old germinating seeds of WT, *FLZ13*-OE, *FLZ13*-OE/*abi5-8*, *ABI5*-OE, and *ABI5*-OE/*flz13-1* treated with 0.5 μM ABA were cross-linked with 1% formaldehyde. The chromatin was then extracted and sheared to approximately 500 base pairs by sonication before being immunoprecipitated with a GFP-Trap (ChromoTek). After cross-linking was reversed, the amount of each precipitated DNA fragment was determined by quantitative PCR. The relative quantity was calculated using the $2^{-\Delta\Delta Ct}$ method and presented as the ratio of immunoprecipitation (IP) to input. Primer pairs used in the ChIP–qPCR assay are listed in Supplemental Table 14.

EMSA

EMSA was performed as described previously (Li et al., 2022b). In brief, full-length ABI5 and FLZ13 were separately fused with a His-MBP tag at the C terminus to generate His-MBP-ABI5 and His-MBP-FLZ13 vectors. The resulting vectors were transformed into *E. coli BL21* (DE3) strains to express the recombinant proteins at 25°C for 6 h with 0.4 mM isopropyl β-D-1-thiogalactopyranoside (IPTG) induction. The expressed proteins were purified from the soluble fractions using His-Magic beads (Sangon Biotech). Biotin-labeled DNA probes were purchased from Sangon Biotech (Shanghai, China) and are listed in Supplemental Table 14. The EMSA was performed using a non-radioactive electrophoretic mobility shift assay kit (Viagene Biotech) following the manufacturer's instructions.

Protein detection and phosphorylation analysis

To analyze the protein levels of FLZ13 and ABI5 during seed germination and their response to ABA, 100 seeds of *pFLZ13::FLZ13-GFP* #9 were surface sterilized and then cold stratified at 4°C in the dark for 3 days before being sown on ½ MS medium plates with or without 0.5 μM ABA. The plates were placed in a growth chamber at 22°C under LD conditions for germination, and the seeds were harvested at the indicated time points. To check the protein levels of ABI5, 100 seeds of WT, *flz13-1*, and *flz13-2* were surface sterilized and then cold stratified at 4°C in the dark for 3 days before being sown on ½ MS medium plates with or without 0.5 μM ABA. The plates were placed in a growth chamber at 22°C under LD conditions for germination, and the seeds were harvested after incubation for 3 days. To check the protein levels of ABI5-GFP, 7-day-old *ABI5*-OE and *ABI5*-OE/*flz13-1* were exposed to 100 μM ABA for 6 h before being harvested. Total protein was extracted from the harvested samples using 20 mM Tris–HCl [pH 7.5], 150 mM NaCl, 1 mM EDTA, 1% Triton X-100, and 1× protease inhibitor cocktail (Roche Diagnostics). The primary antibodies used in this study were anti-ABI5 (Stone et al., 2006; 1:3000 dilution), anti-GFP (HT801-02; 1:2000 dilution), anti-MBP (TransGen, HT701-02; 1:3000 dilution), anti-GST (TransGen, HT601-02; 1:3000 dilution), and anti-H3 (Abcam, ab1791; 1:5000 dilution).

For phosphorylation analysis of ABI5-GFP, 7-day-old *ABI5*-OE and *ABI5*-OE/*flz13-1* plants were exposed to 100 μM ABA for 6 h before being harvested for protein isolation. The ABI5-GFP proteins were purified by GFP-Trap (ChromoTek) and then subjected to phosphorylation analysis using a Phos-tag Biotin BTL-111 kit as described previously (Li et al., 2019).

Data processing and statistical analysis

Histograms with average values and standard deviations were constructed using GraphPad Prism software, and the original data are presented in Supplemental Table 15. Unprocessed images of the western blots are shown in Supplemental Figure 10. ImageJ was used to quantify blot signals. Statistical differences were calculated using one-way analysis of variance (ANOVA) in SPSS software or two-tailed Student's *t*-test in Microsoft Excel. Different letters indicate means that are significantly different according to Tukey's multiple comparison test ($P < 0.05$). *$P < 0.05$.

SUPPLEMENTAL INFORMATION

Supplemental information is available at *Plant Communications Online*.

FUNDING

This work was supported by grants from the Open Competition Program of Top Ten Critical Priorities of Agricultural Science and Technology Innovation for the 14th Five-Year Plan of Guangdong Province (2022SDZG05) and the National Natural Science Foundation of China (32270291, 32061160467, 31870171) to C.G.; the Youth Innovation Promotion Association, Chinese Academy of Sciences (2023364), the Guangdong Basic and Applied Basic Research Foundation (2022A1515012319), and the Guangzhou Basic and Applied Basic Research Foundation (2023A04J0094) to C.Y.; the Sub-Project of Chinese Academy of Sciences Pilot Project (XDA24030502) and the Guangdong Provincial Special Fund for Modern Agriculture Industry Technology Innovation Teams (2020KJ148) to Y.W.; and the National Natural Science Foundation of China (32170362), the Guangdong Natural Science Funds for Distinguished Young Scholars (2022B1515020026), the Youth Innovation Promotion Association, Chinese Academy of Sciences (Y2021094), and the Fund of South China Botanical Garden, Chinese Academy of Sciences (QNXM-02) to M.L.

AUTHOR CONTRIBUTIONS

C.Y., C.G., Y.W., and M.L. conceived of the project and designed the experiments. C.Y., X.L., S.C., C.L., L.Y., K.L., J.L., X.Z., and H.L. performed the experiments. C.Y., C.G., Y.L., S.Z., X.Z., P.R., Y.W., and M.L. analyzed the results. C.Y., C.G., Y.L., X.Z., P.R., Y.W., and M.L. wrote and edited the manuscript. All authors have read and approved the manuscript.

ACKNOWLEDGMENTS

We thank Faqiang Li (South China Agricultural University) and Richard Vierstra (University of Wisconsin, Madison) for providing ABI5 antibody. No conflict of interest is declared.

Received: December 5, 2022
Revised: May 5, 2023
Accepted: June 6, 2023
Published: June 9, 2023

REFERENCES

Addicott, F.T., Lyon, J.L., Ohkuma, K., Thiessen, W.E., Carns, H.R., Smith, O.E., Cornforth, J.W., Milborrow, B.V., Ryback, G., and Wareing, P.F. (1968). Abscisic acid: a new name for abscisin II (dormin). Science **159**:1493. https://doi.org/10.1126/science.159.3822.1493.b.

Branon, T.C., Bosch, J.A., Sanchez, A.D., Udeshi, N.D., Svinkina, T., Carr, S.A., Feldman, J.L., Perrimon, N., and Ting, A.Y. (2018). Efficient proximity labeling in living cells and organisms with TurboID. Nat. Biotechnol. **36**:880–887. https://doi.org/10.1038/nbt.4201.

Brocard, I.M., Lynch, T.J., and Finkelstein, R.R. (2002). Regulation and role of the Arabidopsis abscisic acid-insensitive 5 gene in abscisic acid, sugar, and stress response. Plant Physiol. **129**:1533–1543. https://doi.org/10.1104/pp.005793.

Carles, C., Bies-Etheve, N., Aspart, L., Léon-Kloosterziel, K.M., Koornneef, M., Echeverria, M., and Delseny, M. (2002). Regulation of Arabidopsis thaliana Em genes: role of ABI5. Plant J. **30**:373–383. https://doi.org/10.1046/j.1365-313x.2002.01295.x.

Chen, K., Li, G.J., Bressan, R.A., Song, C.P., Zhu, J.K., and Zhao, Y. (2020). Abscisic acid dynamics, signaling, and functions in plants. J. Integr. Plant Biol. **62**:25–54. https://doi.org/10.1111/jipb.12899.

Chen, S., Li, X., Yang, C., Yan, W., Liu, C., Tang, X., and Gao, C. (2021). Genome-wide identification and characterization of FCS-like zinc finger (FLZ) family genes in maize (Zea mays) and functional analysis of ZmFLZ25 in plant abscisic acid response. Int. J. Mol. Sci. **22**:3529. https://doi.org/10.3390/ijms22073529.

Clough, S.J., and Bent, A.F. (1998). Floral dip: a simplified method for Agrobacterium-mediated transformation of Arabidopsis thaliana. Plant J. **16**:735–743. https://doi.org/10.1046/j.1365-313x.1998.00343.x.

Cornforth, J.W., Milborrow, B.V., Ryback, G., and Wareing, P.F. (1965). Chemistry and physiology of 'Dormins' in sycamore: identity of sycamore 'dormin' with abscisin II. Nature **205**:1269–1270. https://doi.org/10.1038/2051269b0.

Cutler, S.R., Rodriguez, P.L., Finkelstein, R.R., and Abrams, S.R. (2010). Abscisic acid: emergence of a core signaling network. Annu. Rev. Plant Biol. **61**:651–679. https://doi.org/10.1146/annurev-arplant-042809-112122.

De Giorgi, J., Piskurewicz, U., Loubery, S., Utz-Pugin, A., Bailly, C., Mène-Saffrané, L., and Lopez-Molina, L. (2015). An endosperm-associated cuticle is required for Arabidopsis seed viability, dormancy and early control of germination. PLoS Genet. **11**, e1005708. https://doi.org/10.1371/journal.pgen.1005708.

Eagles, C.F., and Wareing, P.F. (1963). Dormancy regulators in woody plants: experimental induction of dormancy in betula pubescens. Nature **199**:874–875. https://doi.org/10.1038/199874a0.

Finkelstein, R., Gampala, S.S.L., Lynch, T.J., Thomas, T.L., and Rock, C.D. (2005). Redundant and distinct functions of the ABA response loci ABA-INSENSITIVE(ABI)5 and ABRE-BINDING FACTOR (ABF)3. Plant Mol. Biol. **59**:253–267. https://doi.org/10.1007/s11103-005-8767-2.

Finkelstein, R.R. (1994). Mutations at two new Arabidopsis ABA response loci are similar to the abi3 mutations. Plant J. **5**:765–771. https://doi.org/10.1046/j.1365-313X.1994.5060765.x.

Finkelstein, R.R., and Lynch, T.J. (2000). The Arabidopsis abscisic acid response gene ABI5 encodes a basic leucine zipper transcription factor. Plant Cell **12**:599–609. https://doi.org/10.1105/tpc.12.4.599.

Fujii, H., and Zhu, J.K. (2009). Arabidopsis mutant deficient in 3 abscisic acid-activated protein kinases reveals critical roles in growth, reproduction, and stress. Proc. Natl. Acad. Sci. USA **106**:8380–8385. https://doi.org/10.1073/pnas.0903144106.

Fujii, H., Verslues, P.E., and Zhu, J.K. (2007). Identification of two protein kinases required for abscisic acid regulation of seed germination, root growth, and gene expression in Arabidopsis. Plant Cell **19**:485–494. https://doi.org/10.1105/tpc.106.048538.

Furihata, T., Maruyama, K., Fujita, Y., Umezawa, T., Yoshida, R., Shinozaki, K., and Yamaguchi-Shinozaki, K. (2006). Abscisic acid-dependent multisite phosphorylation regulates the activity of a transcription activator AREB1. Proc. Natl. Acad. Sci. USA **103**:1988–1993. https://doi.org/10.1073/pnas.0505667103.

Franks, R.G., Wang, C., Levin, J.Z., and Liu, Z. (2002). SEUSS, a member of a novel family of plant regulatory proteins, represses floral homeotic gene expression with LEUNIG. Development **129**:253–263. https://doi.org/10.1242/dev.129.1.253.

Gampala, S.S.L., Finkelstein, R.R., Sun, S.S.M., and Rock, C.D. (2002). ABI5 interacts with abscisic acid signaling effectors in rice protoplasts. J. Biol. Chem. **277**:1689–1694. https://doi.org/10.1074/jbc.M109980200.

Garcia, M.E., Lynch, T., Peeters, J., Snowden, C., and Finkelstein, R. (2008). A small plant-specific protein family of ABI five binding proteins (AFPs) regulates stress response in germinating Arabidopsis seeds and seedlings. Plant Mol. Biol. **67**:643–658. https://doi.org/10.1007/s11103-008-9344-2.

Gendrel, A.V., Lippman, Z., Martienssen, R., and Colot, V. (2005). Profiling histone modification patterns in plants using genomic tiling microarrays. Nat. Methods **2**:213–218. https://doi.org/10.1038/nmeth0305-213.

Gonzalez-Guzman, M., Pizzio, G.A., Antoni, R., Vera-Sirera, F., Merilo, E., Bassel, G.W., Fernández, M.A., Holdsworth, M.J., Perez-Amador, M.A., Kollist, H., and Rodriguez, P.L. (2012). Arabidopsis PYR/PYL/RCAR receptors play a major role in quantitative regulation of stomatal aperture and transcriptional response to abscisic acid. Plant Cell **24**:2483–2496. https://doi.org/10.1105/tpc.112.098574.

Guo, P., Chong, L., Wu, F., Hsu, C.C., Li, C., Zhu, J.K., and Zhu, Y. (2021). Mediator tail module subunits MED16 and MED25 differentially regulate abscisic acid signaling in Arabidopsis. J. Integr. Plant Biol. **63**:802–815. https://doi.org/10.1111/jipb.13062.

Hamburger, D., Rezzonico, E., MacDonald-Comber Petétot, J., Somerville, C., and Poirier, Y. (2002). Identification and characterization of the Arabidopsis PHO1 gene involved in phosphate loading to the xylem. Plant Cell **14**:889–902. https://doi.org/10.1105/tpc.000745.

He, Y., Tang, W., Swain, J.D., Green, A.L., Jack, T.P., and Gan, S. (2001). Networking senescence-regulating pathways by using Arabidopsis enhancer trap lines. Plant Physiol. **126**:707–716. https://doi.org/10.1104/pp.126.2.707.

He, Y., and Gan, S. (2004). A novel zinc-finger protein with a proline-rich domain mediates ABA-regulated seed dormancy in Arabidopsis. Plant Mol. Biol. **54**:1–9. https://doi.org/10.1023/B:PLAN.0000028730.10834.e3.

Holdsworth, M.J., Bentsink, L., and Soppe, W.J.J. (2008). Molecular networks regulating Arabidopsis seed maturation, after-ripening, dormancy and germination. New Phytol. **179**:33–54. https://doi.org/10.1111/j.1469-8137.2008.02437.x.

Hu, Y., Han, X., Yang, M., Zhang, M., Pan, J., and Yu, D. (2019). The transcription factor INDUCER OF CBF EXPRESSION1 interacts with ABSCISIC ACID INSENSITIVE5 and DELLA proteins to fine-tune abscisic acid signaling during seed germination in Arabidopsis. Plant Cell **31**:1520–1538. https://doi.org/10.1105/tpc.18.00825.

Huang, D.W., Sherman, B.T., and Lempicki, R.A. (2009). Systematic and integrative analysis of large gene lists using DAVID bioinformatics resources. Nat. Protoc. **4**:44–57. https://doi.org/10.1038/nprot.2008.211.

Huang, Y., Sun, M.M., Ye, Q., Wu, X.Q., Wu, W.H., and Chen, Y.F. (2017). Abscisic acid modulates seed germination via ABA INSENSITIVE5-mediated PHOSPHATE1. Plant Physiol. **175**:1661–1668. https://doi.org/10.1104/pp.17.00164.

Jamsheer K, M., and Laxmi, A. (2015). Expression of Arabidopsis FCS-Like Zinc finger genes is differentially regulated by sugars, cellular energy level, and abiotic stress. Front. Plant Sci. **6**:746. https://doi.org/10.3389/fpls.2015.00746.

Jamsheer K, M., Sharma, M., Singh, D., Mannully, C.T., Jindal, S., Shukla, B.N., and Laxmi, A. (2018). FCS-like zinc finger 6 and 10 repress SnRK1 signalling in Arabidopsis. Plant J. **94**:232–245. https://doi.org/10.1111/tpj.13854.

Jamsheer K, M., Jindal, S., Sharma, M., Awasthi, P., S, S., Sharma, M., Mannully, C.T., and Laxmi, A. (2022). A negative feedback loop of TOR signaling balances growth and stress-response trade-offs in plants. Cell Rep. **39**, 110631. https://doi.org/10.1016/j.celrep.2022.110631.

Ju, L., Jing, Y., Shi, P., Liu, J., Chen, J., Yan, J., Chu, J., Chen, K.M., and Sun, J. (2019). JAZ proteins modulate seed germination through interaction with ABI5 in bread wheat and Arabidopsis. New Phytol. **223**:246–260. https://doi.org/10.1111/nph.15757.

Katsuta, S., Masuda, G., Bak, H., Shinozawa, A., Kamiyama, Y., Umezawa, T., Takezawa, D., Yotsui, I., Taji, T., and Sakata, Y. (2020). Arabidopsis Raf-like kinases act as positive regulators of subclass III SnRK2 in osmostress signaling. Plant J. **103**:634–644. https://doi.org/10.1111/tpj.14756.

Kobayashi, Y., Murata, M., Minami, H., Yamamoto, S., Kagaya, Y., Hobo, T., Yamamoto, A., and Hattori, T. (2005). Abscisic acid-activated SNRK2 protein kinases function in the gene-regulation pathway of ABA signal transduction by phosphorylating ABA response element-binding factors. Plant J. **44**:939–949. https://doi.org/10.1111/j.1365-313X.2005.02583.x.

Lee, K.P., Piskurewicz, U., Turečková, V., Carat, S., Chappuis, R., Strnad, M., Fankhauser, C., and Lopez-Molina, L. (2012). Spatially and genetically distinct control of seed germination by phytochromes A and B. Genes Dev. **26**:1984–1996. https://doi.org/10.1101/gad.194266.112.

Lee, S.C., and Luan, S. (2012). ABA signal transduction at the crossroad of biotic and abiotic stress responses. Plant Cell Environ. **35**:53–60. https://doi.org/10.1111/j.1365-3040.2011.02426.x.

Leung, J., and Giraudat, J. (1998). Abscisic acid signal transduction. Annu. Rev. Plant Physiol. Plant Mol. Biol. **49**:199–222. https://doi.org/10.1146/annurev.arplant.49.1.199.

Li, H., Wei, J., Liao, Y., Cheng, X., Yang, S., Zhuang, X., Zhang, Z., Shen, W., and Gao, C. (2022a). MLKs kinases phosphorylate the ESCRT component FREE1 to suppress abscisic acid sensitivity of seedling establishment. Plant Cell Environ. **45**:2004–2018. https://doi.org/10.1111/pce.14336.

Li, H., Li, Y., Zhao, Q., Li, T., Wei, J., Li, B., Shen, W., Yang, C., Zeng, Y., Rodriguez, P.L., et al. (2019). The plant ESCRT component FREE1 shuttles to the nucleus to attenuate abscisic acid signalling. Nat. Plants **5**:512–524. https://doi.org/10.1038/s41477-019-0400-5.

Li, X., Huang, Y., Han, Y., Yang, Q., Zheng, Y., Li, W., Shen, W., Yang, C., and Gao, C. (2022b). Arabidopsis flowering integrator SOC1 transcriptionally regulates autophagy in response to long-term carbon starvation. J. Exp. Bot. **73**:6589–6599. https://doi.org/10.1093/jxb/erac298.

Lim, S., Park, J., Lee, N., Jeong, J., Toh, S., Watanabe, A., Kim, J., Kang, H., Kim, D.H., Kawakami, N., and Choi, G. (2013). ABA-insensitive3, ABA-insensitive5, and DELLAs Interact to activate the expression of SOMNUS and other high-temperature-inducible genes in imbibed seeds in Arabidopsis. Plant Cell **25**:4863–4878. https://doi.org/10.1105/tpc.113.118604.

Lin, Z., Li, Y., Wang, Y., Liu, X., Ma, L., Zhang, Z., Mu, C., Zhang, Y., Peng, L., Xie, S., et al. (2021). Initiation and amplification of SnRK2 activation in abscisic acid signaling. Nat. Commun. **12**:2456. https://doi.org/10.1038/s41467-021-22812-x.

Long, J.A., Ohno, C., Smith, Z.R., and Meyerowitz, E.M. (2006). TOPLESS regulates apical embryonic fate in Arabidopsis. Science **312**:1520–1523. https://doi.org/10.1126/science.1123841.

Lopez-Molina, L., and Chua, N.H. (2000). A null mutation in a bZIP factor confers ABA-insensitivity in Arabidopsis thaliana. Plant Cell Physiol. **41**:541–547. https://doi.org/10.1093/pcp/41.5.541.

Lopez-Molina, L., Mongrand, S., and Chua, N.H. (2001). A postgermination developmental arrest checkpoint is mediated by abscisic acid and requires the ABI5 transcription factor in Arabidopsis. Proc. Natl. Acad. Sci. USA **98**:4782–4787. https://doi.org/10.1073/pnas.081594298.

Lopez-Molina, L., Mongrand, S., McLachlin, D.T., Chait, B.T., and Chua, N.H. (2002). ABI5 acts downstream of ABI3 to execute an ABA-dependent growth arrest during germination. Plant J. **32**:317–328. https://doi.org/10.1046/j.1365-313x.2002.01430.x.

Lopez-Molina, L., Mongrand, S., Kinoshita, N., and Chua, N.H. (2003). AFP is a novel negative regulator of ABA signaling that promotes ABI5 protein degradation. Genes Dev. **17**:410–418. https://doi.org/10.1101/gad.1055803.

Ma, Y., Szostkiewicz, I., Korte, A., Moes, D., Yang, Y., Christmann, A., and Grill, E. (2009). Regulators of PP2C phosphatase activity function as abscisic acid sensors. Science **324**:1064–1068. https://doi.org/10.1126/science.1172408.

Manfre, A.J., Lanni, L.M., and Marcotte, W.R., Jr. (2006). The Arabidopsis group 1 LATE EMBRYOGENESIS ABUNDANT protein ATEM6 is required for normal seed development. Plant Physiol. **140**:140–149. https://doi.org/10.1104/pp.105.072967.

Mair, A., Xu, S.L., Branon, T.C., Ting, A.Y., and Bergmann, D.C. (2019). Proximity labeling of protein complexes and cell-type-specific organellar proteomes in Arabidopsis enabled by TurboID. Elife **8**, e47864. https://doi.org/10.7554/eLife.47864.

Miyazono, K.I., Miyakawa, T., Sawano, Y., Kubota, K., Kang, H.J., Asano, A., Miyauchi, Y., Takahashi, M., Zhi, Y., Fujita, Y., et al. (2009). Structural basis of abscisic acid signalling. Nature **462**:609–614. https://doi.org/10.1038/nature08583.

Nakabayashi, K., Okamoto, M., Koshiba, T., Kamiya, Y., and Nambara, E. (2005). Genome-wide profiling of stored mRNA in Arabidopsis thaliana seed germination: epigenetic and genetic regulation of transcription in seed. Plant J. **41**:697–709. https://doi.org/10.1111/j.1365-313X.2005.02337.x.

Nakamura, S., Lynch, T.J., and Finkelstein, R.R. (2001). Physical interactions between ABA response loci of Arabidopsis. Plant J. **26**:627–635. https://doi.org/10.1046/j.1365-313x.2001.01069.x.

Nakashima, K., Fujita, Y., Kanamori, N., Katagiri, T., Umezawa, T., Kidokoro, S., Maruyama, K., Yoshida, T., Ishiyama, K., Kobayashi, M., et al. (2009). Three Arabidopsis SnRK2 protein kinases, SRK2D/SnRK2.2, SRK2E/SnRK2.6/OST1 and SRK2I/SnRK2.3, involved in ABA signaling are essential for the control of seed development and dormancy. Plant Cell Physiol. **50**:1345–1363. https://doi.org/10.1093/pcp/pcp083.

Nguyen, Q.T.C., Lee, S.J., Choi, S.W., Na, Y.J., Song, M.R., Hoang, Q.T.N., Sim, S.Y., Kim, M.S., Kim, J.I., Soh, M.S., and Kim, S.Y. (2019). Arabidopsis Raf-like kinase Raf10 is a regulatory component of core ABA signaling. Mol. Cells **42**:646–660. https://doi.org/10.14348/molcells.2019.0173.

Nishimura, N., Hitomi, K., Arvai, A.S., Rambo, R.P., Hitomi, C., Cutler, S.R., Schroeder, J.I., and Getzoff, E.D. (2009). Structural mechanism of abscisic acid binding and signaling by dimeric PYR1. Science **326**:1373–1379. https://doi.org/10.1126/science.1181829.

O'Malley, R.C., Huang, S.S.C., Song, L., Lewsey, M.G., Bartlett, A., Nery, J.R., Galli, M., Gallavotti, A., and Ecker, J.R. (2016). Cistrome and epicistrome features shape the regulatory DNA landscape. Cell **165**:1280–1292. https://doi.org/10.1016/j.cell.2016.04.038.

Ohkuma, K., Lyon, J.L., Addicott, F.T., and Smith, O.E. (1963). Abscisin II, an abscission-accelerating substance from Young cotton fruit. Science **142**:1592–1593. https://doi.org/10.1126/science.142.3599.1592.

Pan, J., Wang, H., Hu, Y., and Yu, D. (2018). Arabidopsis VQ18 and VQ26 proteins interact with ABI5 transcription factor to negatively modulate ABA response during seed germination. Plant J. **95**:529–544. https://doi.org/10.1111/tpj.13969.

Park, S.Y., Fung, P., Nishimura, N., Jensen, D.R., Fujii, H., Zhao, Y., Lumba, S., Santiago, J., Rodrigues, A., Chow, T.F.F., et al. (2009). Abscisic acid inhibits type 2C protein phosphatases via the PYR/PYL family of START proteins. Science **324**:1068–1071. https://doi.org/10.1126/science.1173041.

Ran, X., Zhao, F., Wang, Y., Liu, J., Zhuang, Y., Ye, L., Qi, M., Cheng, J., and Zhang, Y. (2020). Plant Regulomics: a data-driven interface for retrieving upstream regulators from plant multi-omics data. Plant J. **101**:237–248. https://doi.org/10.1111/tpj.14526.

Reeves, W.M., Lynch, T.J., Mobin, R., and Finkelstein, R.R. (2011). Direct targets of the transcription factors ABA-Insensitive(ABI)4 and ABI5 reveal synergistic action by ABI4 and several bZIP ABA response factors. Plant Mol. Biol. **75**:347–363. https://doi.org/10.1007/s11103-011-9733-9.

Santiago, J., Dupeux, F., Round, A., Antoni, R., Park, S.Y., Jamin, M., Cutler, S.R., Rodriguez, P.L., and Márquez, J.A. (2009). The abscisic acid receptor PYR1 in complex with abscisic acid. Nature **462**:665–668. https://doi.org/10.1038/nature08591.

Saruhashi, M., Kumar Ghosh, T., Arai, K., Ishizaki, Y., Hagiwara, K., Komatsu, K., Shiwa, Y., Izumikawa, K., Yoshikawa, H., Umezawa, T., et al. (2015). Plant Raf-like kinase integrates abscisic acid and hyperosmotic stress signaling upstream of SNF1-related protein kinase2. Proc. Natl. Acad. Sci. USA **112**:E6388–E6396. https://doi.org/10.1073/pnas.1511238112.

Skubacz, A., Daszkowska-Golec, A., and Szarejko, I. (2016). The role and regulation of ABI5 (ABA-Insensitive 5) in plant development, abiotic stress responses and phytohormone crosstalk. Front. Plant Sci. **7**:1884. https://doi.org/10.3389/fpls.2016.01884.

Stone, S.L., Williams, L.A., Farmer, L.M., Vierstra, R.D., and Callis, J. (2006). KEEP ON GOING, a RING E3 ligase essential for Arabidopsis growth and development, is involved in abscisic acid signaling. Plant Cell **18**:3415–3428. https://doi.org/10.1105/tpc.106.046532.

Takahashi, Y., Zhang, J., Hsu, P.K., Ceciliato, P.H.O., Zhang, L., Dubeaux, G., Munemasa, S., Ge, C., Zhao, Y., Hauser, F., and Schroeder, J.I. (2020). MAP3 Kinase-dependent SnRK2-kinase activation is required for abscisic acid signal transduction and rapid osmotic stress response. Nat. Commun. **11**:12. https://doi.org/10.1038/s41467-019-13875-y.

Tyanova, S., Temu, T., Sinitcyn, P., Carlson, A., Hein, M.Y., Geiger, T., Mann, M., and Cox, J. (2016). The Perseus computational platform for comprehensive analysis of (prote)omics data. Nat. Methods **13**:731–740. https://doi.org/10.1038/nmeth.3901.

Xing, H.L., Dong, L., Wang, Z.P., Zhang, H.Y., Han, C.Y., Liu, B., Wang, X.C., and Chen, Q.J. (2014). A CRISPR/Cas9 toolkit for multiplex genome editing in plants. BMC Plant Biol. **14**:327. https://doi.org/10.1186/s12870-014-0327-y.

Yang, C., Ma, Y., He, Y., Tian, Z., and Li, J. (2018). OsOFP19 modulates plant architecture by integrating the cell division pattern and brassinosteroid signaling. Plant J. **93**:489–501. https://doi.org/10.1111/tpj.13793.

Yang, C., Shen, W., Yang, L., Sun, Y., Li, X., Lai, M., Wei, J., Wang, C., Xu, Y., Li, F., et al. (2020). HY5-HDA9 module transcriptionally regulates plant autophagy in response to light-to-dark conversion and nitrogen starvation. Mol. Plant **13**:515–531. https://doi.org/10.1016/j.molp.2020.02.011.

Yang, M., Han, X., Yang, J., Jiang, Y., and Hu, Y. (2021). The Arabidopsis circadian clock protein PRR5 interacts with and stimulates ABI5 to modulate abscisic acid signaling during seed germination. Plant Cell **33**:3022–3041. https://doi.org/10.1093/plcell/koab168.

Yu, F., Wu, Y., and Xie, Q. (2015). Precise protein post-translational modifications modulate ABI5 activity. Trends Plant Sci. **20**:569–575. https://doi.org/10.1016/j.tplants.2015.05.004.

Zhao, X., Dou, L., Gong, Z., Wang, X., and Mao, T. (2019). BES1 hinders ABSCISIC ACID INSENSITIVE5 and promotes seed germination in Arabidopsis. New Phytol. **221**:908–918. https://doi.org/10.1111/nph.15437.

Zhou, X., Hao, H., Zhang, Y., Bai, Y., Zhu, W., Qin, Y., Yuan, F., Zhao, F., Wang, M., Hu, J., et al. (2015). SOS2-LIKE PROTEIN KINASE5, an SNF1-RELATED PROTEIN KINASE3-type protein kinase, is important for abscisic acid responses in Arabidopsis through phosphorylation of ABSCISIC ACID-INSENSITIVE5. Plant Physiol. **168**:659–676. https://doi.org/10.1104/pp.114.255455.

Zhou, Y., Zhou, B., Pache, L., Chang, M., Khodabakhshi, A.H., Tanaseichuk, O., Benner, C., and Chanda, S.K. (2019). Metascape provides a biologist-oriented resource for the analysis of systems-level datasets. Nat. Commun. **10**:1523. https://doi.org/10.1038/s41467-019-09234-6.

Plant Communications, Volume *4*

Supplemental information

ABI5–FLZ13 module transcriptionally represses growth-related genes to delay seed germination in response to ABA

Chao Yang, Xibao Li, Shunquan Chen, Chuanliang Liu, Lianming Yang, Kailin Li, Jun Liao, Xuanang Zheng, Hongbo Li, Yongqing Li, Shaohua Zeng, Xiaohong Zhuang, Pedro L. Rodriguez, Ming Luo, Ying Wang, and Caiji Gao

ABI5-FLZ13 Module Transcriptionally Represses Growth-related Genes to Delay Seed Germination in Response to ABA

Chao Yang[1,2,*] Xibao Li[2], Shunquan Chen[2], Chuanliang Liu[2], Lianming Yang[2], Kailin Li[2], Jun Liao[2], Xuanang Zheng[2], Hongbo Li[2], Yongqing Li[1], Shaohua Zeng[1], Xiaohong Zhuang[3], Pedro L. Rodriguez[4], Ming Luo[1,*], Ying Wang[1,*] and Caiji Gao[2,*]

[1]Key Laboratory of South China Agricultural Plant Molecular Analysis and Genetic Improvement & Guangdong Provincial Key Laboratory of Applied Botany, South China Botanical Garden, Chinese Academy of Sciences, Guangzhou, 510650, China

[2]Guangdong Provincial Key Laboratory of Biotechnology for Plant Development, School of Life Sciences, South China Normal University (SCNU), Guangzhou 510631, China

[3]School of Life Sciences, Centre for Cell and Developmental Biology, The Chinese University of Hong Kong, Shatin, New Territories, Hong Kong, China

[4]Instituto de Biología Molecular y Celular de Plantas, Consejo Superior de Investigaciones Científicas-Universidad Politécnica de Valencia, 46022 Valencia, Spain

*** Correspondence: Chao Yang (chaoyang@scbg.ac.cn), Ming Luo (luoming@scbg.ac.cn), Ying Wang (yingwang@scib.ac.cn) , Caiji Gao (gaocaiji@m.scnu.edu.cn)**

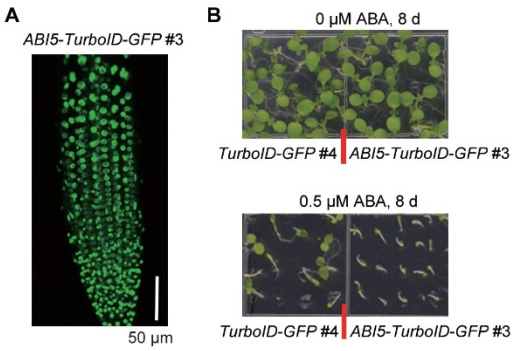

Supplemental Figure 1. Characterization of *ABI5-TurboID-GFP* transgenic plants.

A, Confocal image showing the nuclear localization of ABI5-TurboID-GFP proteins in root cells of 5-day-old seedlings.

B, Photographs of seedlings of *TurboID-GFP* #4 and *ABI5-TurboID-GFP* #3 upon 0 or 0.5 μM ABA treatment for 8 days.

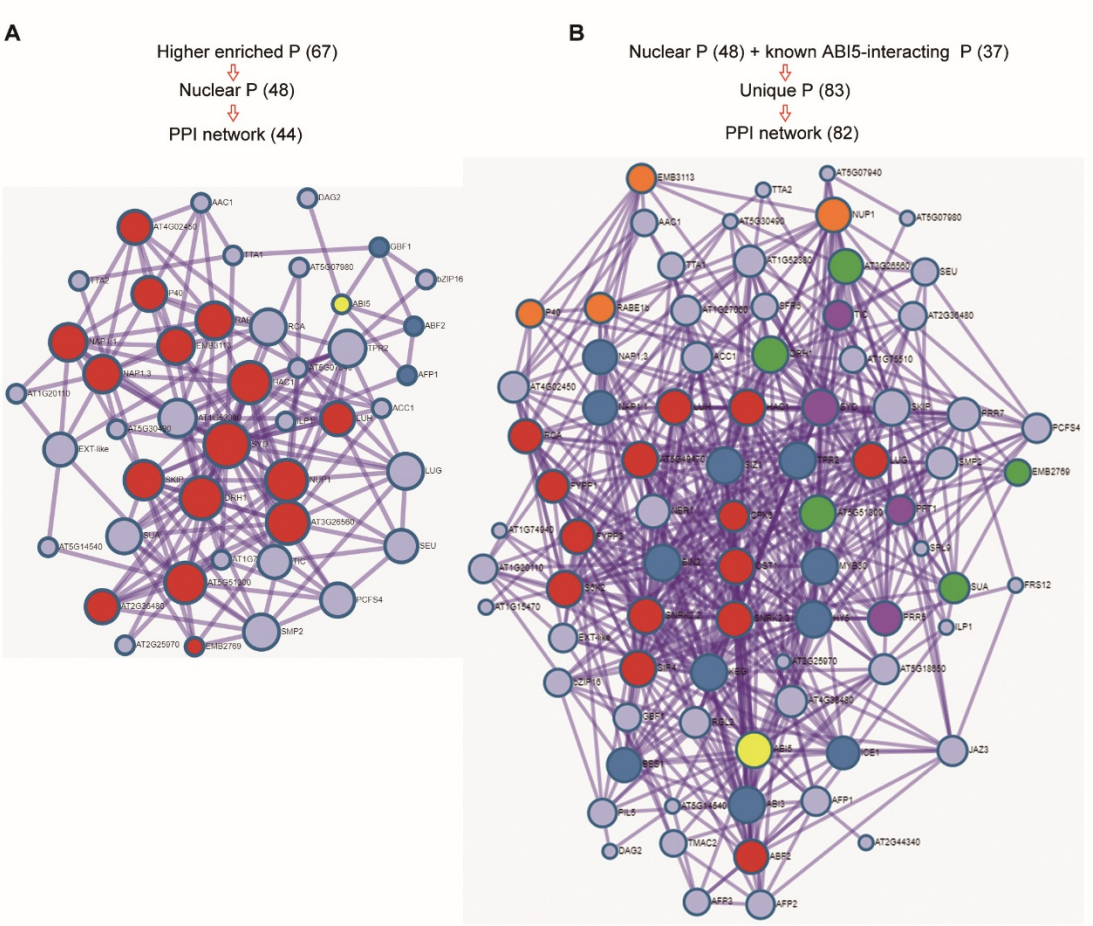

Supplemental Figure 2. Metascape visualization of ABI5 interactome networks. The numbers for the checked proteins are shown on the top. The protein-protein interaction (PPI) networks were generated on line (https://metascape.org/; Zhou et al., 2019). Each node represents a protein and each line represents the interlink between two proteins. ABI5 is highlighted in yellow. P, Protein.

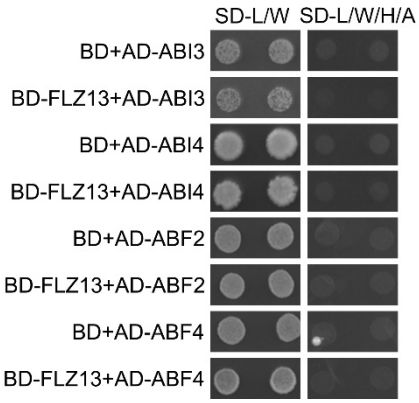

Supplemental Figure 3. Y2H analysis of the interaction between FLZ13 and other key transcription factors involved in ABA signaling.

Protein interaction were determined by growth of the yeast cells co-transformed with various combinations of the plasmids on synthetic dropout medium lacking Leu and Trp (SD-L/W) and lacking Leu, Trp, His, and adenine (SD-L/W/H/A) as indicated.

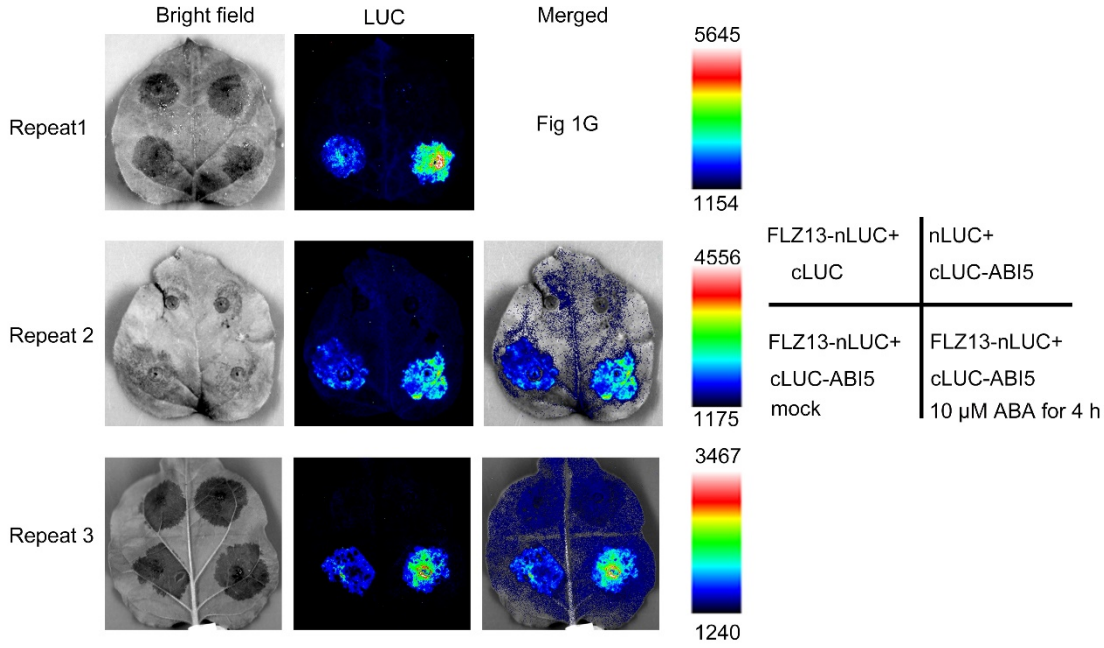

Supplemental Figure 4. Three biological replications of LCI experiments showing that ABA promotes FLZ13-ABI5 interaction.

Three independent experiments of LCI showing the interaction between FLZ13 and ABI5, and the promoting effects of ABA on this interaction. *Agrobacteria* harboring FLZ13-nLUC was co-infiltrated with *Agrobacteria* harboring cLUC-ABI5 into *N. benthamiana* leaves. The FLZ13-nLUC/cLUC and cLUC-ABI5/nLUC pairs were used as negative controls. After 36 h co-infiltration, leaves were treated with mock and 10 μM ABA for 4 h followed by luminescence imaging.

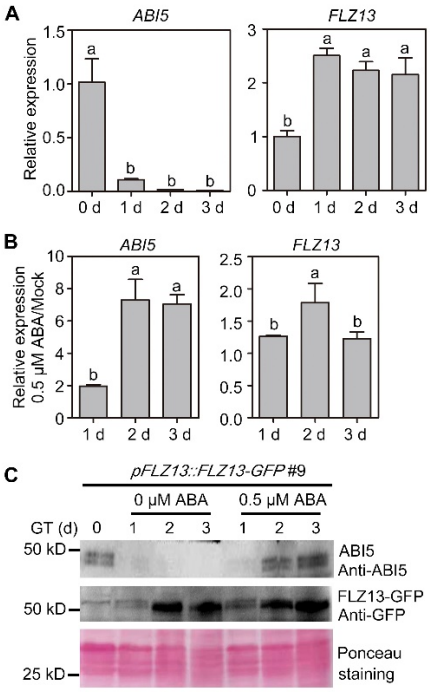

Supplemental Figure 5. Expression pattern of *FLZ13* and *ABI5* during seed germination with or without ABA treatment.

A, Quantitative RT-PCR assay showing the expression of *FLZ13* and *ABI5* in dry and germinating seeds. *Actin2* was used as the internal control. Data are presented as mean ± SD (*n* = 3 technical replicates). The different letters above each bar indicate statistically significant differences determined by one-way ANOVA followed by Tukey's multiple comparison test ($P < 0.05$). This experiment was repeated twice and similar results were obtained.

B, Quantitative RT-PCR assay showing the expression of *FLZ13* and *ABI5* in germinating seeds in response to ABA treatment. The data are presented as the ratio of ABA to Mock treatment. *Actin2* was used as the internal control. Data are presented as mean ± SD (*n* = 3 technical replicates). The different letters above each bar indicate statistically significant differences determined by one-way ANOVA followed by Tukey's multiple comparison test ($P < 0.05$). This experiment was repeated twice and similar results were obtained.

C, Immunoblot analysis of FLZ13-GFP and ABI5 proteins in response to ABA treatment during seed germination. GT: germination time.

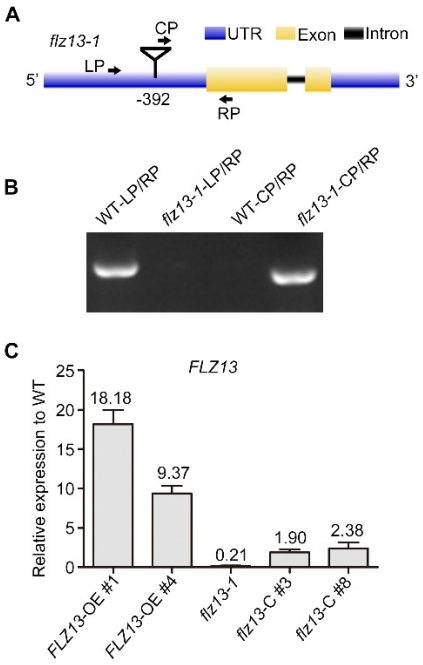

Supplemental Figure 6. Characterization of *FLZ13*-related plant materials.

A, Schematic gene structure of *FLZ13*. Triangle indicates the T-DNA insertion site in *flz13-1* mutant. Arrows indicate primers used for genotyping of *flz13-1* mutant. LP, left primer; CP, common primer; RP, right primer; UTR, untranslated regions.

B, Gel electrophoresis of genotyping PCR with WT and *flz13-1* DNA using primers indicated in panel A.

C, Quantitative RT-PCR showing the gene expression of *FLZ13* in the indicated genetic background. Data are presented as mean ± SD (*n* = 3 technical replicates). *Actin2* was used as the internal control. The expression level in WT was set as 1.0. The numbers on the bars indicate the fold change.

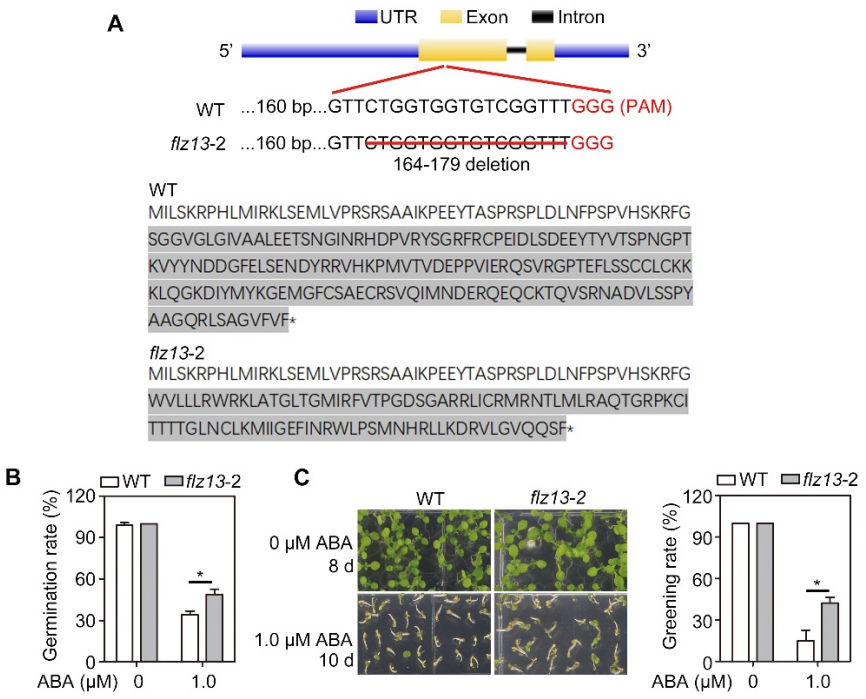

Supplemental Figure 7. Characterization of the *flz13*-2 mutant.

A, The CRISPR/Cas9 gene editing mutant of *FLZ13*. *flz13*-2 harbors a 16-nucleotides deletion which is predicted to encode a truncated protein. UTR, untranslated regions; PAM, protospacer adjacent motif.

B, Germination rates of WT and *flz13-2* treated with the indicated concentrations of ABA. The germination rates were recorded 3 d after plating on 1/2 MS medium. Data are presented as mean ± SD (*n* = 3 biological replicates). The asterisk indicates statistically significant differences (*$P < 0.05$) determined by Student's *t*-test.

C, Photographs of seedlings (left) and greening rates (right) of WT and *flz13*-2 upon 0 or 1.0 μM ABA treatment as recorded at the indicated time points. Data is mean ± SD (*n* = 3 biological replicates). The asterisk indicates statistically significant differences (*$P < 0.05$) determined by Student's *t*-test.

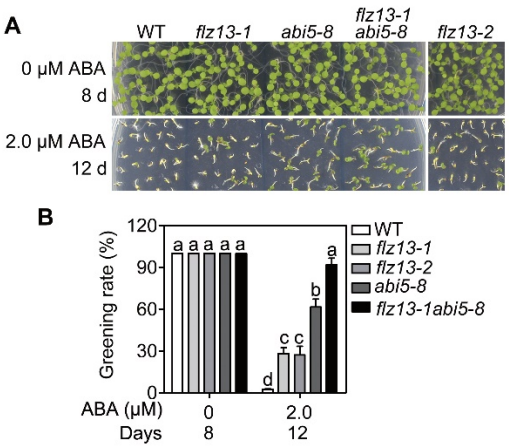

Supplemental Figure 8. ABA response of *flz13* and *abi5* mutants.

A, Photographs of seedlings of WT, *flz13-1*, *flz13*-2, *abi5-8*, and *flz13-1 abi5-8* upon 0 or 2.0 μM ABA treatment at the indicated time points.

B, Cotyledon greening rates of WT, *flz13-1*, *flz13*-2, *abi5-8*, and *flz13-1 abi5-8* upon various concentration ABA treatment at the indicated time points. Data are presented as mean ± SD (*n* = 3 biological replicates for 0 μM ABA treatment and *n* = 4 biological replicates for 2.0 μM ABA treatment). The different letters above each bar indicate statistically significant differences determined by one-way ANOVA followed by Tukey's multiple comparison test ($P < 0.05$).

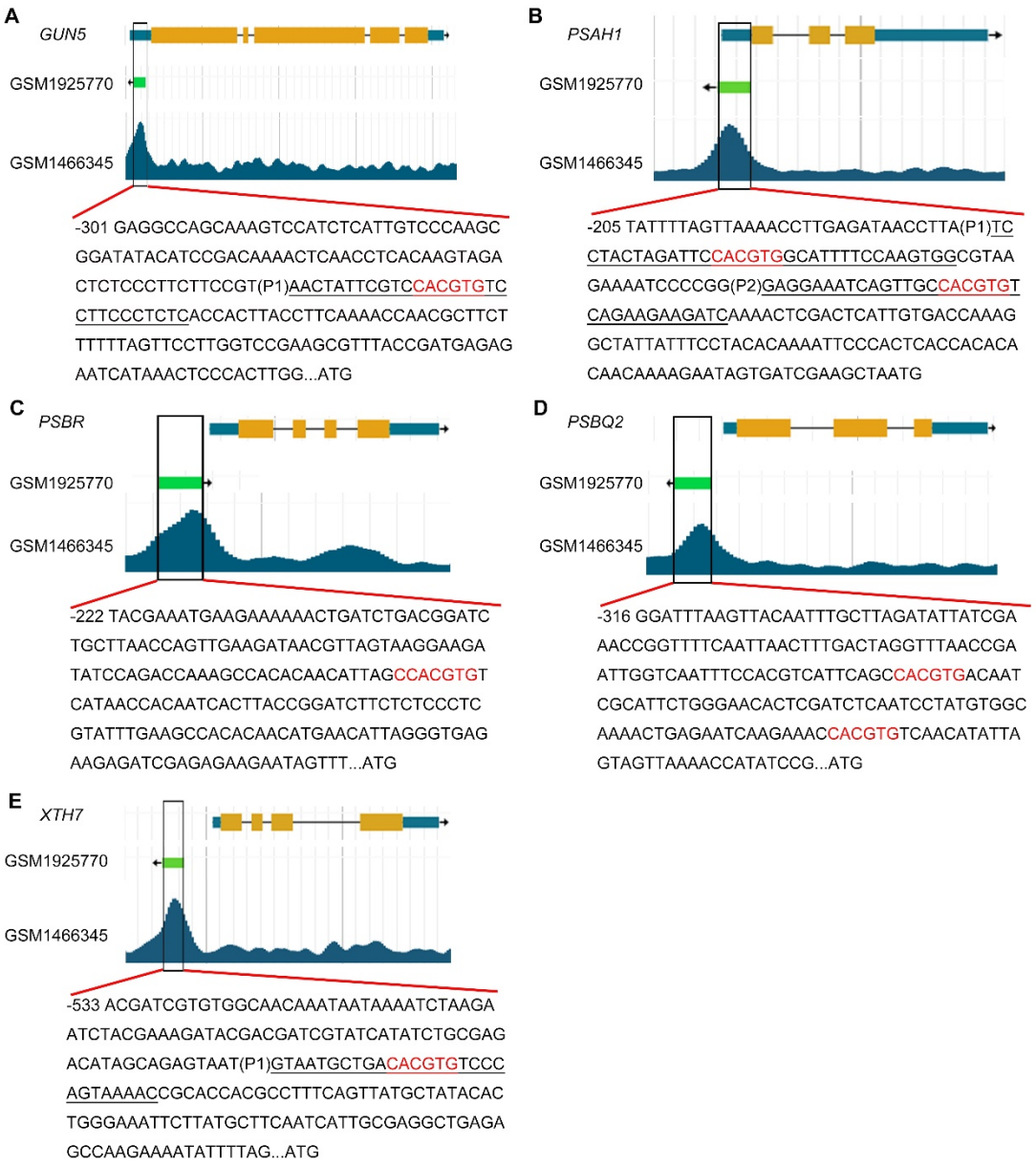

Supplemental Figure 9. Five selected target genes of ABI5.

The raw data were downloaded from http://bioinfo.sibs.ac.cn/plant-regulomics/ (Ran et al., 2020) and edited in photoshop. The primers used for EMSA analysis are underlined. The sequences of G-box are highlighted in red.

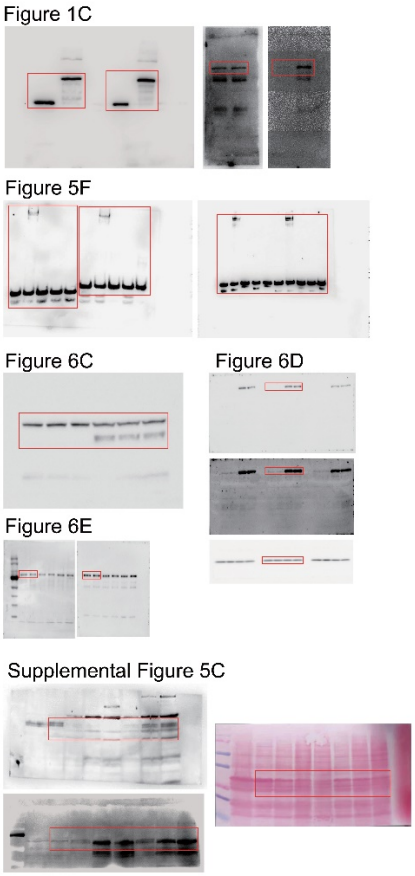

Supplemental Figure 10. Original images for Western blots. The red boxes mark the sheared regions presented in the corresponding figures.

Supplemental Tables

The following materials are available in the uploaded Excel file.

Supplemental Table 1. List of the higher enriched proteins in ABI5-TurboID-GFP vs. TurboID-GFP comparison.

Supplemental Table 2. List of the 48 nuclear-localized proteins of 67 identified higher enriched ones in Supplemental Table 1.

Supplemental Table 3. List of the 37 known ABI5-interacting proteins.

Supplemental Table 4. DEGs in response to ABA treatment in WT germinating seeds.

Supplemental Table 5. Expression of known ABA-induced marker genes in the RNA-seq data.

Supplemental Table 6. DEGs in ABI5-OE seeds compared to WT upon ABA treatment.

Supplemental Table 7. DEGs in FLZ13-OE seeds compared to WT upon ABA treatment.

Supplemental Table 8. Expression of 567 ABA, FLZ13 and ABI5 co-regulated genes.

Supplemental Table 9. GO enrichment of 496 ABA/ABI5/FLZ13 co-repressed genes.

Supplemental Table 10. Target genes of ABI5.

Supplemental Table 11. List of the 35 ABI5 target genes co-regulated by ABA/ABI5/FLZ13.

Supplemental Table 12. Expression of the 500 ABA/ABI5/FLZ13 synchronously co-regulated genes in WT, *FLZ13*-OE, and *FLZ13*-OE/*abi5-8* plants upon ABA treatment.

Supplemental Table 13. Expression of the 500 synchronously ABA/ABI5/FLZ13 co-regulated genes in WT, *ABI5*-OE, and *ABI5*-OE/*flz13-1* plants upon ABA treatment.

Supplemental Table 14. List of primers used in this study.

Supplemental Table 15. Original data for bar charts production and statistical analysis.